Published in final edited form as:
AJR Am J Roentgenol. 2012 August ; 199(2): 278–291. doi:10.2214/AJR.12.8816.

Molecular Imaging of Prostate Cancer: PET Radiotracers

Hossein Jadvar[1]

[1]Department of Radiology, Keck School of Medicine of USC, University of Southern California, 2250 Alcazar St, CSC 102, Los Angeles, CA 90033

Abstract

OBJECTIVE—Recent advances in the fundamental understanding of the complex biology of prostate cancer have provided an increasing number of potential targets for imaging and treatment. The imaging evaluation of prostate cancer needs to be tailored to the various phases of this remarkably heterogeneous disease.

CONCLUSION—In this article, I review the current state of affairs on a range of PET radiotracers for potential use in the imaging evaluation of men with prostate cancer.

Keywords

cancer; CT; MRI; PET; prostate

The complex and heterogeneous biology of prostate cancer poses major challenges and opportunities. The disease is a major public health problem and is associated with significant emotional, comorbid practical, and economic costs. There is also an evolution in the development and use of specific endpoints for the emerging therapeutic approaches with the general goal to control, relieve, or eliminate disease manifestations (e.g., prostate-specific antigen [PSA], imaging findings, and symptoms) and to delay or prevent future disease manifestations [1]. Currently, imaging plays an important role in many aspects of this disease, but its role will need to evolve to accurately answer key clinical questions at various phases of the disease in a cost-effective manner. These clinical decision-making landmarks include accurate primary diagnosis, characterization and staging of cancer at the time of initial presentation, determination of local recurrence or distant disease at the time of biochemical recurrence of prostate cancer to select the most appropriate therapy, accurate assessment of therapy response to various treatment regimen under the new practice paradigm, and prediction of patient outcome (e.g., time-to-event endpoints such as time to hormone refractoriness in castrate-sensitive disease, time to progression, and overall survival).

The parallel advances in deciphering the molecular biology underpinnings of prostate cancer and the development of new imaging biomarkers and integrated imaging systems have provided unprecedented new and exciting opportunities to address these pivotal clinical needs. The biologically relevant targets for imaging may include metabolites (e.g., glucose, fatty acids, and amino acids), antigens (e.g., prostate-specific membrane antigen and prostate-specific stem cell antigen), androgen signaling (e.g., androgen receptor), angiogenesis, hypoxia, and gene-based pathways [2–21].

Address correspondence to H. Jadvar (jadvar@usc.edu).

PET is fundamentally suited for the imaging evaluation of biologic targets and events. With the ever-increasing availability and access to hybrid PET/CT scanners, as well as the recent emergence of PET/MRI systems coupled with exceptional ongoing research and development in radiochemistry, the future for noninvasive molecular imaging–based examination of prostate cancer biology not only will lead to new enlightening levels of understanding of the disease but also will be clinically useful. With these introductory remarks in mind, I review the current evidence on the potential utility of a number of PET radiotracers in the imaging evaluation of prostate cancer.

Glucose Metabolism: ^{18}F-FDG

A recognized hallmark of malignancy is the Warburg effect, which involves complex adaptive biologic mechanisms for enhanced cancer cell survival [22, 23]. PET with FDG takes advantage of this phenomenon and has excelled in the imaging evaluation of cancer [24]. Increased expression of cellular membrane glucose transporters and enhanced hexokinase enzymatic activity have been noted in many cancers that display augmented glucose metabolism [25, 26].

Effert et al. [27] assessed the expression of glucose transporter 1 (GLUT1) messenger RNA in hormone-independent and -sensitive prostate cancer cell lines. GLUT1 expression was higher in poorly differentiated hormone-independent cell lines than in well-differentiated hormone-sensitive cell lines. GLUT1 gene expression has also been shown to be generally higher in prostate cancer than in benign prostatic hyperplasia [28]. A recent study showed that overexpression of GLUT1 was observed in only some of the highly proliferative intraductal prostate cancers and that the expression level was generally low in most prostate tumors, probably reflecting the well-recognized heterogeneity of prostate tumor biology [29]. Xenograft prostate cancer mouse models have shown that androgen deprivation can significantly decrease the accumulation of FDG in hormone-sensitive tumors but it may not exert a significant effect on hormone-independent tumors [30–32].

Evaluation of the prostate gland on FDG PET/CT studies is challenging because of overlap of FDG uptake in normal, benign, and malignant tissues; the multifocal distribution of cancer deposits mixed with noncancerous cells; and the proximity of the gland to the urinary bladder. Despite these general limitations, one retrospective study assessed the level of FDG uptake in the “normal” prostate gland of men who had undergone FDG PET/CT without known or clinically suspected prostate disease [33]. Mean and maximum standardized uptake values (SUVs) were (mean ± SD) 1.3 ± 0.4 (range, 0.1–2.7) and 1.6 ± 0.4 (range, 1.1–3.7), respectively.

FDG PET generally has a limited role in the primary diagnosis and staging of prostate cancer in view of overlap of tracer accumulation in normal and abnormal prostate tissues [34]. Shiiba et al. [35] used a time-of-flight PET/CT to correlate the FDG uptake in primary prostate cancer with the biopsy specimen’s Gleason score. The cutoff SUV_{max}, sensitivity, and specificity for differentiating between biopsy specimens with a summed Gleason score of 5 or less and specimens with a summed Gleason score of 6 or greater were 2.8, 61.7%, and 80.0%, respectively. Another study reported a sensitivity of 80% and a positive predictive value of 87% for detection of prostate tumors with Gleason score of 7 and greater in men who presented with more than an intermediate risk of prostate cancer according to elevated serum PSA level [36]. Han and colleagues [37] evaluated the clinical significance of incidental focal prostate FDG uptake in men without known prostate cancer. The incidence of focal prostatic FDG uptake was 1.2%. Of the 55 cases that had clinical follow-up, only three had confirmed malignancy by biopsy, with SUV_{max} values of 2.3, 3.3, and 3.6; the remaining 52 cases were declared benign, with a mean SUV_{max} of 3.2 ± 1.7, which

overlapped significantly with the malignant cases. These studies suggest that, in some cases, FDG PET may be able to characterize prostate tumors of sufficient size, which then can be helpful in imaging-directed biopsy of clinically relevant lesions [38].

The experience with FDG PET in the imaging evaluation of men with biochemical failure after definitive therapy for primary prostate cancer is quite limited. Biochemical failure is defined as an increase in serum PSA level with negative standard imaging studies after definitive therapy for primary prostate cancer. The American Urologic Association defines biochemical recurrence in postprostatectomy patients as an initial serum PSA level of 0.2 ng/mL or higher, with a second confirmatory level higher than 0.2 ng/mL [39]. In patients with prior primary external beam radiotherapy, the American Society for Therapeutic Radiology and Oncology consensus definition for biochemical failure recommends an increase of 2 ng/ mL or more above the nadir PSA level, regardless of hormonal therapy [40]. In one investigation, of 91 men with PSA relapse after prostatectomy, FDG PET detected local or systemic disease in 31% of patients with PSA relapse [41]. However, the validation criteria used in some cases included other positive standard imaging that violated the definition of PSA relapse–only clinical state [11]. In another study, FDG PET had sensitivity, specificity, positive predictive value, and negative predictive value of 75%, 100%, 100%, and 67.7%, respectively, for the detection of pelvic lymph node metastases, with histopathologic examination of the surgically harvested nodes for validation [42]. Recently, my colleagues and I [43] provided evidence in a prospective clinical study that FDG PET/CT plays a much more limited role than previously reported in the imaging evaluation of men with PSA relapse (range, 0.5–40.2 ng/mL) and strictly negative standard imaging studies.

In men with metastatic prostate cancer, FDG PET/CT may distinguish between metabolically active osseous lesions and metabolically dormant lesions, and the concordance of FDG PET/CT with other imaging studies appears to be higher in castrate-resistant metastatic disease than in castrate-sensitive disease [44–47]. FDG PET/CT may be useful in the evaluation of treatment response in metastatic prostate cancer, similar to the experience with many other cancers, with favorable response portrayed as therapy-induced decline in FDG uptake of tumor sites in comparison with the pretreatment scan [48, 49] (Fig. 1). However, again similar to the experience with other cancers, the response may be heterogeneous with the finding of significant decline in metabolic activity at some tumor sites but not in others. There may also be differences in imaging-based treatment response assessment depending on the response criteria used [50]. With regard to clinical impact, recent data analysis from the National Oncologic PET Registry in the United States has found that FDG PET/CT may indeed have a major impact on the clinical management of up to 35% of men with prostate cancer, mostly prompting treatment when none was planned before the PET scan [51]. Similar to other cancers, higher tumor FDG uptake in prostate tumor appears to be associated with poorer prognosis in comparison with tumors with lower metabolic activity [52, 53].

In summary, FDG PET/CT is generally limited in the primary diagnosis, staging, and restaging of prostate cancer. However, it may be useful in tumor characterization and in assessment of treatment response and prognosis in castrate-sensitive and castrate-resistant metastatic prostate cancer.

Lipogenesis

Acetate

Acetate is a simple metabolite that is preferentially transported across the cellular membrane through the monocarboxylate transporter. The two major sources of acetate consumption are

the Krebs cycle and the metabolic pathways related to the production of phospholipids in cellular membranes facilitated by the fatty acid synthase reaction [54–56]. Preclinical studies have confirmed malignancy-induced up-regulation of fatty acid synthase as the underlying biologic basis for the enhanced ^{11}C-acetate uptake in prostate cancer [57, 58].

Normal biodistribution of ^{11}C-acetate displays high accumulation in the pancreas, variable uptake in the liver and bowel, and some renal uptake with little urinary excretion [59]. A three-compartment three-parameter model describes the acetate kinetics in prostate cancer adequately [60]. Similar to FDG and choline, there can be a considerable overlap among the uptake levels in primary cancer, benign prostatic hyperplasia, and normal prostate gland, but generally, the tracer uptake appears to be greater in the tumor than in the normal and benign prostatic hyperplasia tissue [61].

Limited number of comparative studies have shown that ^{11}C-acetate may be more sensitive than FDG in detection of primary and metastatic prostate cancer, although overall the tracers appear to be complementary [62, 63]. ^{11}C-acetate may be useful in the detection of tumor recurrence in men who had been previously treated for their primary disease, with lesion detectability of up to 75% [64, 65]. The success rate for lesion detection by ^{11}C-acetate appeared to be related to serum PSA level, with a 59% positive rate in patients with serum PSA level greater than 3 ng/mL that declined significantly to 4% in patients with serum PSA levels 3 ng/mL or lower [66].

An ^{18}F-labeled formulation of acetate has also been reported with potential use in prostate cancer, although experience with this tracer remains scant [67]. A comparative animal study of ^{11}C-acetate and ^{18}F-fluoroacetate showed that, for most organs, the tumor-to-organ uptake ratios at 30 minutes after tracer administration were higher with ^{18}F-fluoroacetate than with ^{11}C-acetate, whereas the tumor-to-heart and tumor-to-prostate ratios were similar [68]. A recent investigation in cynomolgus monkeys and pigs showed that ^{18}F-fluoroacetate is not a functional analog of ^{11}C-acetate in normal physiology, with ^{18}F-fluoroacetate showing relatively protracted blood retention, rapid clearance from liver, excretion in bile and urine, and defluorination (i.e., high bone uptake) [69]. Finally, in a limited study that compared ^{11}C-acetate and ^{11}C-choline, the tracers appeared to be similarly useful in imaging prostate cancer in individual patients [70].

Choline

Choline is a water-soluble essential nutrient that was discovered in 1864 by Adolph Strecker. Choline enters the cell through choline transporters and is the precursor for the biosynthesis of phospholipids, which are major components of the cellular membrane. The biologic basis for the accumulation of radiolabeled choline in tumors is, in part, due to overexpression of choline kinase in support of malignancy-induced increased demand for cellular membrane synthesis. Choline kinase catalyzes the phosphorylation of choline to form phosphorylcholine, followed by generation of phosphatidylcholine in the tumor cell membrane [71, 72]. Choline uptake in prostate tumor appears to be affected by hypoxia but may be uncorrelated to cellular proliferation [73, 74].

Initial studies with choline were performed with ^{11}C as the radiolabel [75]. Normal biodistribution of ^{11}C-choline shows relatively high accumulation in the pancreas, liver, kidneys, and salivary glands; variable uptake in the bowel; and little urinary excretion, with the last feature advantageous for the assessment of the prostate gland. Scher et al. [76] reported sensitivity of 87% and specificity of 62% for the detection of primary prostate cancer with histopathologic examination as the reference standard. Another similar investigation found a lower sensitivity of 66% and a higher specificity of 81% for localization of primary prostate cancer based on a sextant histopathologic analysis [77].

When ^{11}C-choline was compared with transrectal ultrasound, both PET and transrectal ultrasound tended to understage the disease [78]. To reduce the partial volume effect, Martorana et al. [79] assessed the diagnostic performance of ^{11}C-choline PET/ CT for prostate nodules 5 mm or larger in men with suspected prostate cancer before the 12-core standard transrectal ultrasound–guided prostate biopsy. Although PET had a relatively high sensitivity (83%) for detection of cancer, its sensitivity for assessment of extraprostatic extension was quite low (22%). Given the range of reported detection rates with ^{11}C-choline PET/CT, a rational query may be whether the detection rate is associated with relevant parameters, such as tumor grade, location, size, and PSA level. For example, it has been noted that tumor configuration may affect detectability (unifocal, 49%; multifocal, 21%; and rindlike, 11%) [80]. Giovacchini and colleagues [81] reported no significant correlation between lesion SUV_{max}, PSA level, and Gleason score on a patient-based analysis.

A study of the comparative diagnostic performance of ^{11}C-choline PET/CT, MRI, and MR spectroscopy for detection of primary prostate cancer, with histologic analysis as the reference standard, had sensitivity and specificity of 55% and 86%, respectively, for PET/ CT, 54% and 75% for MRI, and 81% and 67% for MR spectroscopy [82]. A similar investigation reported sensitivity of 100% for ^{11}C-choline PET, 60% for MRI, and 65% for MR spectroscopy [83]. Eschmann et al. [84] compared ^{11}C-choline PET/CT with whole-body MRI for staging of prostate cancer with histologic analysis and follow-up for validation criteria. The sensitivity and specificity were 97% and 77%, respectively, for ^{11}C-choline PET and 79% and 94% for whole-body MRI. These results suggested that PET and MRI might provide complementary diagnostic information. With the recent development of sophisticated image fusion software, integrated PET/MRI whole-body imaging systems, high-field MRI, and multiparametric MRI techniques (e.g., diffusion-weighted imaging and dynamic contrast enhancement), there may be opportunities for synergism between PET and MRI for more accurate detection and staging of primary prostate cancer [85–87].

Considering the cumulative experience with ^{11}C- and ^{18}F-choline PET, the overall reported sensitivity ranges between 38% and 98% for the detection of locally recurrent and metastatic disease in men with biochemical recurrence of prostate cancer [88–92]. The wide range of sensitivity may relate to the heterogeneity of patient population in terms of PSA level ranges, type of primary therapy, and the type and quality of validation criteria. For example, in one study, ^{11}C-choline was determined to localize recurrence in a higher percentage of men after primary radiation therapy than after radical prostatectomy (78% vs 38%) [93]. In another study, the sensitivity and specificity of ^{11}C-choline PET/CT for the detection of local recurrence after radical prostatectomy were 73% and 88%, respectively [94]. Scattoni et al. [95] reported sensitivity of 64% and specificity of 90% for detection of nodal metastases in men with PSA relapse after radical retropubic prostatectomy.

The detection rate of choline PET may be associated with the PSA level or the other PSA-derived parameters. Therefore, many investigations have focused on this potential relationship to identify a “trigger” PSA level to decipher when patients should be considered for imaging evaluation with choline PET. Unfortunately, many studies have not used the strict requirement for negative standard imaging results. Thus, the unique contribution of choline PET in this clinical setting has become blurred. Despite this limitation, the general notion has been that higher PSA levels, higher PSA velocity, and shorter PSA doubling times may be associated with higher detection rate on choline PET, probably reflecting the amount of tumor burden available for detection.

Krause et al. [90] reported ^{11}C-choline detection rates of 36% for PSA levels less than 1 ng/ mL, 43% for PSA levels 1–2 ng/mL, 62% for PSA levels 2–3 ng/mL, and 73% for PSA levels 3 ng/mL or higher. Castellucci et al. [96] evaluated the likelihood of lesion detection

on ^{11}C-choline PET/CT in 190 men after radical prostatectomy who presented with PSA relapse in the 0.2–25.4 ng/mL range. The likelihood of lesion detection was increased with PSA levels higher than 2.4 ng/ mL and with PSA doubling times of less than 3.4 months or PSA velocities of higher than 1 ng/mL/y when the PSA levels were less than 2.4 ng/mL. In another investigation, ^{11}C-choline and FDG PET were both used in detecting disease in 73 men with PSA relapse [97]. Validation was by biopsy or increase in PSA without therapy and decrease in PSA after therapy. At all PSA levels, ^{11}C-choline had twice higher sensitivity of 60.6%, in comparison with 31% for FDG. In a recent report, Picchio et al. [98] compared ^{11}C-choline PET/CT and standard bone scintigraphy for the detection of bone metastases in 78 men with biochemical progression of disease (PSA level, 0.2–500 ng/mL). The findings on each scan were designated as positive, negative, or equivocal for malignancy, and then the diagnostic performance of the imaging studies were assessed twice, once with equivocal findings as true-positive and once as true-negative. The ranges of sensitivity and specificity were 89–89% and 98–100%, respectively, for ^{11}C-choline and 100–70% and 75–100% for bone scintigraphy. The authors concluded that ^{11}C-choline and bone scintigraphy are complementary, with the former offering higher specificity and the latter providing higher sensitivity. Also in that study, the diagnostic performance of ^{11}C-choline PET/CT was not affected by androgen deprivation therapy. Conversely, another group of researchers showed that androgen deprivation therapy significantly and concordantly reduces PSA levels and ^{11}C-choline uptake in men with castrate-sensitive prostate cancer [99]. The latter observation of an androgen effect on choline uptake in patients was in line with the recently reported in vitro cell line studies [32].

DeGrado et al. [100] reported the synthesis of an ^{18}F-labeled formulation of choline. Over the past decade, ^{18}F-fluorocholine has received much attention given the advantages of the longer half-life of ^{18}F in comparison with that of ^{11}C [101]. Preclinical studies have found high ^{18}F-fluorocholine uptake in prostate cancer with little effect from castration [102, 103].

Normal biodistribution of ^{18}F-fluorocholine shows relatively high uptake in the pancreas, liver, spleen, and kidneys; variable uptake in the bowel; and excretion into urine. Similar to FDG and ^{11}C acetate, the uptake of ^{18}F-fluorocholine overlaps among normal, benign, and malignant prostate tissues [104]. Also similar to the case with ^{11}C-choline, there are mixed results, with the potential utility of ^{18}F-fluorocholine in the diagnosis and staging of primary prostate cancer [105]. Beheshti et al. [106] performed ^{18}F-fluorocholine PET/ CT in men with clinically organ-confined tumor but who were at intermediate (PSA level, 10–20 ng/ mL; Gleason score, 7) and high (PSA level, > 20 ng/mL; Gleason score, ≥ 8) risk for extracapsular extension before undergoing radical prostatectomy with extended pelvic lymph node dissection. The sensitivity, specificity, positive predictive value, and negative predictive value of ^{18}F-fluorocholine for the detection of pelvic lymphadenopathy were 45%, 96%, 82%, and 83%, respectively, for all lymph node sizes and 66%, 96%, 82%, and 92% for lymph nodes 5 mm or larger (i.e., nodes larger than the PET spatial resolution limitation). In general, however, although there is no established role for ^{18}F-fluorocholine PET in the initial diagnosis and staging of prostate cancer, the technique may be of some value in imaging-guided investigational treatments (e.g., focal therapy).

Fluorine-18-fluorocholine (similar to ^{11}C-choline) may have a role in the management of men with biochemical recurrence of prostate cancer with a diagnostic performance that appears to improve with increasing PSA level, although it is not recommended for routine use when the PSA level is less than 1 ng/mL [89] (Fig. 2). Pelosi et al. [107] reported a detection rate of 20% for PSA level 1 ng/mL or lower, 44% for PSA level 1–5 ng/ mL, and 82% for PSA level greater than 5 ng/mL. Another investigation showed a 41% true-positive rate in restaging patients with PSA levels less than 5 ng/mL [108]. A recent report determined the relationship between PSA kinetics and ^{18}F-fluorocholine PET/CT detection

rate in 82 men with biochemical recurrence of prostate cancer after total prostatectomy [109]. The median PSA level was significantly higher in PET-positive than PET-negative patients (4.3 vs 1.0 ng/mL; $p < 0.01$). A PSA level of 1.74 ng/ mL was determined to be the optimal PSA threshold for detection of recurrent prostate cancer, with a sensitivity of 82% and specificity of 74%. Moreover, the median PSA velocity was significantly higher for PET-positive than PET-negative patients (6.4 vs 1.1 ng/mL/y; $p < 0.01$) with an optimal threshold of 1.27 ng/mL/y. On a similar theme, Schillaci et al. [110] recommended that ^{18}F-fluorocholine PET/CT may be considered in men with PSA level greater than 2 ng/mL, PSA doubling time of 6 months or less, and PSA velocity greater than 2 ng/mL/y.

Langsteger et al. [111] compared ^{18}F-fluorocholine PET/CT and ^{18}F-NaF PET/CT for the detection of bone metastases in 40 men with primary or recurrent prostate cancer. A lesion-based comparison showed no significant difference. A patient-based comparison found the same sensitivity of 91% for both ^{18}F-fluorocholine and ^{18}F-NaF but higher specificity of 89% for ^{18}F-fluorocholine, in comparison with 83% for ^{18}F-NaF. Although that study suggested that ^{18}F-fluorocholine PET/CT may be able to replace ^{18}F-NaF PET/CT, another report [112] concluded that combined imaging may be most useful for management decisions and accurate treatment response assessment. Beheshti et al. [113] correlated the uptake of ^{18}F-fluorocholine in bone metastases to the morphologic changes on CT. Lytic lesions showed higher choline uptake than did blastic lesions (average SUV_{max}, 11 ± 3.2 for lytic lesions vs 7.8 ± 3.0 for blastic lesions). Hormonal therapy did not significantly affect the choline uptake in the osseous lesions. Three PET/CT patterns for bone metastases were identified: those with ^{18}F-fluorocholine uptake only (i.e., bone marrow infiltration without morphologic changes on CT), those with both ^{18}F-fluorocholine uptake and CT morphologic changes, and lesions with no ^{18}F-fluorocholine uptake but high density on CT (nonviable tumor). Similar findings have been observed with FDG PET/CT [114].

Cellular Proliferation

Imaging cellular proliferation provides useful noninvasive diagnostic information about the rate of tumor growth and early assessment of treatment response [115–117]. PET in conjunction with radiotracers that track the thymidine salvage pathway of DNA synthesis has been studied relatively extensively for imaging tumor cellular proliferation [118]. Although ^{11}C-thymidine was an early candidate, its rapid catabolism complicated its kinetic model analysis and limited its practical utility [119–122]. In this section, I review the preclinical and pilot clinical experiences with two major ^{18}F-labeled PET radiotracers in the imaging evaluation of cellular proliferation in prostate cancer.

[Fluorine-18]-3′-Deoxy-3′-Fluorothymidine (FLT)

FLT is phosphorylated by thymidine kinase (TK) 1, which is retained in proliferating cells without DNA incorporation and can be described by a three-compartment kinetic model [123–125]. Recently, Kukuk et al. [31] reported the pharmacokinetics of FLT, FDG, and ^{11}C-choline in two hormone-independent (PC-3 and DU145) and two hormone-dependent (CWR22 and PAC 120) prostate cancer xenograft mouse models using PET. Both FLT and FDG showed the highest uptake in PC-3 hormone-independent tumors. FDG uptake in hormone-dependent CWR22 tumors was also noted to be high but decreased significantly after androgen deprivation therapy. Although, in that study, FLT uptake was insufficient at baseline to provide reliable information on response to therapy, other studies have shown that FLT uptake is markedly reduced after castration or treatment with diethylstilbestrol [126]. A significant decline in FLT uptake has also been noted in the 22Rv1 hormone-refractory prostate tumors implanted in athymic mice in response to docetaxel treatment [127]. Despite these few early encouraging results, the exact role of FLT in the imaging evaluation of response to treatment in men with prostate cancer awaits more

extensive studies. A complicating factor is also the physiologically high level of marrow FLT uptake that can hinder osseous lesion detection and assessment.

[Fluorine-18]-2′-Fluoro-5-Methyl-1-β-D-Arabinofuranosyluracil (FMAU)

FMAU is a thymidine analog that is phosphorylated by TK and incorporated in DNA. FMAU is preferentially phosphorylated by the mitochondrial TK2 in comparison with the cytosolic TK1 [128]. Unlabeled FMAU was originally of clinical interest as an anticancer and an antiviral drug when used in pharmacologic doses [129]. In tracer doses, FMAU can be labeled with ^{11}C or ^{18}F and has been noted to be useful for imaging tumor proliferation [130–134]. FMAU has also been used for imaging reporter gene expression using the herpes simplex virus type 1 TK1 system [135–138]. An automated GMP–compliant radiosynthesis of FMAU has been described recently [139].

Carbon-14-FMAU behaves very similarly to thymidine with respect to cellular uptake velocity, saturability of cellular incorporation, and intracellular metabolite pools and is reflective of tumor cell division [140]. A recent report showed that ^{11}C-FMAU uptake in a dog brain tumor model correlated with tumor growth rate and could be well described by a three-compartment kinetic model [141]. Other researchers have supported the adequacy of a three-compartment model for FMAU [133]. The D-isomer of the compound shows higher accumulation in tumors than those for the L-isomer and FLT [142].

FMAU is resistant to degradation and has very little accumulation in bone and in urinary bladder, which renders it a potentially ideal PET radiotracer for imaging in prostate cancer [143, 144]. There may be an association between androgen signaling and thymidine metabolism, possibly related to the androgen control of mitochondrial function, including TK2 enzymatic activity [145, 146].

Sun et al. [147] showed in a small pilot study that FMAU accumulated in locally recurrent (tumor-to-background pelvis activity ratio, 2.3–6.3) and osseous metastatic sites (tumor-to-background normal bone activity ratio, 2.4–3) of prostate cancer. Moreover, FMAU displayed rapid blood clearance (95% of blood activity cleared within 10 minutes) and stability (about 70% of urine activity as intact FMAU at 60 minutes).

Other substituted 2′-[^{18}F]fluro-2′-deoxy- arabinofuranosyluracil derivates such as 2′-deoxy-2′-[^{18}F]fluoro-5-bromo-1-β-D-arabinofuranosyluracil, 2′-deoxy-2′[^{18}F] fluro-5-chloro-1-β-D-arabinofuranosyluracil, 2′-deoxy-2′-^{18}F-fluoro-5-fluoro-1-β-D-arabinofuranosyluracil, and others have also been synthesized. However, their potential competitive advantage over FLT and FMAU will need further investigation [148, 149].

Receptors

Androgen Receptor (AR)

Androgens are essential for the development, growth, and maintenance of the prostate. The effects of androgens are exerted via the nuclear AR, which is a ligand-dependent (either testosterone or 5α-dihydrotestosterone) transcription activator involved in cellular proliferation and differentiation and is present in all histologic types of prostate tumors, in recurrent carcinoma, and in tumor metastases [150–152]. Almost all patients respond favorably to androgen ablation, but virtually all patients will eventually relapse to a castrate-resistant clinical state, which is believed to occur via bypassing or sensitizing the AR pathway. The factors involved may be AR mutation, such that the receptor is either activated promiscuously or is activated in a ligand-independent manner by amplification of coactivators, activation of oncogenes, as well as autocrine growth factors stimulation [152].

With the recent treatment trials including high-dose testosterone or the use of AR-targeted drugs (e.g., AR antagonist MDV3100), imaging biomarkers directed to the AR seems quite rational [153, 154]. Several ligands for the AR have been developed, including 16β-[^{18}F]fluoro-5α-dihydrotestosterone (^{18}F-FDHT) [155–157]. Larson et al. [158] assessed the in vivo targeting and biokinetics of ^{18}F-FDHT in seven patients with clinically progressive metastatic prostate cancer. The metabolism of ^{18}F-FDHT was rapid, with 80% conversion within 10 minutes to radiolabeled metabolites circulating bound to plasma proteins, with tumor uptake of tracer that was rapid and stable. In another study of 20 men with metastatic prostate cancer, ^{18}F-FDHT PET had a sensitivity of 63%, with a noted decline in tumor uptake level 1 day after treatment with flutamide [159]. Moreover, positive PET studies were significantly associated with higher PSA levels. Pharmacokinetics assessment of ^{18}F-FDHT showed that tumor uptake reached a plateau within 20 minutes and that radiolabeled metabolites were not bound to AR on the basis of in vitro studies with CWR22 cells [160]. Preliminary results from a study comparing ^{18}F-FDHT and FDG has shown that there are AR-predominant, glycolysis-predominant, and AR-glycolysis–concordant states, which may have implications for treatment response and prognosis [161] (Fig. 3). Moreover, despite encouraging antitumor activity with MDV3100 in men with castrate-resistant prostate cancer (e.g., decline in PSA, documented response in soft-tissue disease, stabilization of bone disease, and conversion from unfavorable to favorable circulating tumor cell counts), the MDV3100-induced ^{18}F-FDHT uptake changes in tumor did not necessarily parallel the changes in tumor FDG uptake, suggesting that ^{18}F-FDHT may be a pharmacodynamic marker as opposed to a treatment response marker in this setting [47, 153].

Radiation dosimetry of ^{18}F-FDHT has shown absorbed doses from the lowest level in skin (0.00057 ± 0.000281 cGy/MBq) to the highest level in the urinary bladder wall (0.00868 ± 0.00481 cGy/MBq) with 1–2 hours voiding interval, and an effective dose equivalent of 0.00177 ± 0.000152 cSv/MBq [162]. The maximum recommended administered activity was noted to be 331 MBq (8.9 mCi) to keep the maximum normal-tissue absorbed dose below the recommended maximum permissible dose of 5 cGy per single administration.

Gastrin-Releasing Peptide Receptor (GRPR)

Bombesin is a 14–amino acid analog of the human gastrin-releasing peptide that binds to the GRPR. Because GRPR is overexpressed in prostate cancer, there has been an increasing interest in developing PET radiotracers that target the GRPR [163–173]. In a recent study, ^{68}Ga-labeled bombesin analog AMBA (^{68}Ga-DO-TA-CHCO-Gly-4-aminobenzyl-Gln-Trp-Ala-Val-Gly-His-Leu-Met-NH) was compared with ^{18}F-fluorocholine in nude mice bearing human prostate cancer xenografts [174]. The tumor uptake of ^{68}Ga-AMBA was significantly higher than that with ^{18}F-fluorocholine, suggesting that GRPR-targeted imaging may be superior to choline-based imaging. This and other encouraging results with radiolabeled bombesin analogs suggest a potentially important role in the imaging evaluation of prostate cancer that will deserve additional investigation.

Amino Acid

Carbon-11-Methionine

Tumor uptake of ^{11}C-methionine reflects enhanced amino acid transport and protein synthesis that may be present in malignancy. Relatively few data have been published on the potential utility of ^{11}C-methionine in prostate cancer. In a pilot study of 10 patients with progressive prostate cancer, FDG and ^{11}C-methionine were compared. Although both FDG and ^{11}C-methione were taken up by the selected index lesions, ^{11}C-methionine showed a higher tumor-to-blood ratio, more rapid tumor uptake after tracer administration, and a flatter uptake profile than those for FDG [175]. In a prospective study, 12 patients with PSA

relapse and at least one site of new or increasing disease on conventional imaging (bone scintigraphy, CT, or MRI) underwent both FDG PET and ^{11}C-methione PET [176]. With conventional imaging modalities as the standard of reference, the sensitivities of FDG PET and ^{11}C-methionine were 48% and 72.1%, respectively. The authors also suggested that initial ^{11}C-methione uptake may indicate dormant sites of disease followed by an increase in FDG uptake as the disease progresses, therefore reflecting the time-dependent metabolic cascade of progressive metastatic prostate cancer.

Tóth et al. [177] studied 20 men with high PSA levels (3.49–28.6 ng/mL) and negative prostate biopsies. The true-positive detection rate of primary prostate cancer was 35% for the whole group and 46.7% in the PET-positive group. PET was negative in all five patients with negative repeat prostate biopsies. Therefore, it appears that nonstandard imaging with ^{11}C-methionine, if available, may be useful in this group of men with suspected prostate cancer but negative initial biopsy results. More recently, Shiiba et al. [35] performed a similar study in 20 men with suspected primary prostate cancer comparing ^{11}C-methionine and FDG in relation to the tumor Gleason sum score. The tracer uptake in the prostate gland were recorded by small 100-mm^2 round regions of interest placed at six standard locations in the peripheral zone and four standard locations in the apex of the transitional zone. The Gleason sum scores of tumor specimens were grouped as no grade (Gleason sum score of ≤ 5), low grade (Gleason sum score of 6 or 7), and high grade (Gleason sum score of 8–10). The difference in ^{11}C-methione uptake levels between the no-grade and low-grade groups was statistically significant. For FDG, the difference in uptake levels between the no-grade and high-grade groups was statistically significant. The cut-off SUV_{max} and the corresponding sensitivity and specificity for differentiating between no-grade and low-grade plus high-grade groups were 3.15, 78.7%, and 75.6%, respectively, for ^{11}C-methionene and 3.00, 62.8%, and 78.9% for FDG. For separating no-grade plus low-grade and high-grade groups, the cutoff SUV_{max} and the corresponding sensitivity and specificity were 3.76, 70.1%, and 89.7%, respectively, for ^{11}C-methionine and 3.47%, 62.7%, and 86.3% for FDG.

Anti-1-Amino-3-(^{18}F)-Fluorocyclobuate-1-Carboxylic (Anti-^{18}F-FACBC)

Anti[^{18}F]-FACBC is a synthetic l-leucine analog that has been found to accumulate in prostate cancer with relatively little renal excretion [178]. The tracer accumulation in prostate cancer cells correlates with the expression level of the alanine-, serine-, and cysteine-preferring system–mediated amino acid transport, with the large neutral amino acid transporter as an important transport system in the typical intratumoral acidic microenvironment [179]. It has also been shown that the tracer does not get incorporated into proteins [180]. Schuster et al. [181] described their initial experience with anti-^{18}F-FACBC PET in prostate cancer. Visual analysis detected malignancy in 40 of 48 prostate sextants, in seven of nine pelvic nodal basins, and in all four men with local recurrence (Fig. 4). In another study, investigators compared anti-^{18}F-FACBC PET/ CT with ^{111}In-capromab pendetide SPECT/ CT in 50 men with suspected recurrent prostate cancer after definitive therapy for localized disease and negative standard bone scans [182]. Validation was by a combination of tissue histopathologic analysis, additional imaging, and laboratory and clinical data. The sensitivity and specificity for detection of prostate bed recurrence were 89% and 67%, respectively, for anti-^{18}F-FACBC PET/ CT and 69% and 58% for ^{111}In-capromab pendetide SPECT/CT. For detection of extraprostatic involvement, the sensitivity and specificity were 100% and 100%, respectively, for anti-^{18}F-FACBC PET/CT and 10% and 100% for ^{111}In-capromab pendetide SPECT/ CT. Therefore, anti-^{18}F-FACBC PET/CT was clearly more accurate than ^{111}In-capromab pendetide SPECT/CT, especially for detection of occult extraprostatic sites of disease in men with biochemical failure. A case

study of the potential utility of anti-^{18}F-FACBC PET/CT in guiding prostate bed radiotherapy has also been reported [183].

Bone Matrix

Fluorine-18–Labeled Sodium Fluoride (^{18}F-NaF)

Bone scintigraphy with ^{99m}Tc-based radiotracers grossly underestimates the true prevalence of bone metastasis and does not provide a quantifiable metric for monitoring treatment response [184, 185]. These shortcomings may be overcome with ^{18}F-NaF, which is actually an old tracer approved for clinical use by the U.S. Food and Drug Administration in 1972 [186]. Despite the superior performance of ^{18}F-NaF (i.e., high-quality images with rapid blood clearance and high bone-to-background ratio as well as shorter time from tracer administration to imaging), the tracer was not widely used in view of the technical limitations of gamma cameras with high-energy photon imaging and the scarcity of PET scanners. The situation has now changed, with more widespread availability of PET/CT scanners, commercial regional distribution of PET tracers, and recent shortages of ^{99m}Tc-labeled tracers. The recent decision by the Centers for Medicare & Medicaid Services to reimburse for ^{18}F-NaF PET/CT through the National Oncologic PET Registry to assess the effect of ^{18}F-NaF PET/CT on referring physicians' intended management of patients with known or suspected bone metastases has also contributed to its increased clinical use.

Fluorine-18-NaF is rapidly cleared from plasma in a biexponential manner with essentially all tracer retained by bone after a single pass. The bone uptake is related to chemisorption with exchange of $^{18}F^-$ ion for OH^- ion-on the surface of the hydroxyapatite matrix of bone to form fluoroapatite and migration of $^{18}F^-$ ion into the crystalline matrix of bone. There is minimal binding to serum protein and rapid renal clearance [187, 188]. The "super-scan" uptake pattern in widespread osseous metastatic disease is similar to that of standard bone scintigraphy with little renal tracer localization [189]. Procedure guidelines and dosimetry estimates for ^{18}F-NaF have been published elsewhere [190].

Hsu et al. [191] reported in a preclinical animal model that ^{18}F-NaF PET/CT can be useful in characterizing osseous lesions induced by human prostate cancer. Human studies have shown that, in particular, bone lesions with sclerotic or mixed changes tend to show high ^{18}F-NaF uptake [192]. Even-Sapir and colleagues [193] compared ^{99m}Tc-methylene diphosphonate planar bone scintigraphy, SPECT, ^{18}F-NaF PET, and ^{18}F-NaF PET/CT in 25 men with newly diagnosed prostate cancer with Gleason scores of 8 or higher or PSA levels of 20 ng/mL or higher or nonspecific sclerotic lesions on CT and 19 patients who were referred for evaluation of suspected recurrence or progression of disease. They followed rule-based criteria to categorize lesions as malignant, benign, or equivocal with a follow-up range of 6–15 months for establishing truth. In a patient-based analysis, the sensitivity and specificity were 70% and 57%, respectively, for planar bone scintigraphy, 92% and 82% for multiple-FOV SPECT, 100% and 62% for ^{18}F-NaF PET, and 100% and 100% for ^{18}F-NaF fluoride PET/CT. The high sensitivity and specificity of ^{18}F-NaF PET/CT allows the detection of occult bone metastases that are missed on standard bone scintigraphy, with important implications on patient management. For example recently, my colleagues and I [43] reported a true-positive detection rate of 16.2% for occult osseous metastases in 37 men with biochemical recurrence of prostate cancer who underwent ^{18}F-NaF PET/CT (Fig. 5).

With regard to the use of ^{18}F-NaF in monitoring treatment response, a very recent small pilot study of five patients with castrate-resistant metastatic prostate cancer showed that semiquantitative ^{18}F-NaF PET was more accurate than qualitative comparison of scans in assessing response of bone metastases to 223Ra-chloride (Alpharadin, Algeta) therapy and in correlating better with PSA and alkaline phosphatase changes [194]. Despite potential

advantages of ^{18}F-NaF PET/CT over standard bone scintigraphy in quantification of treatment response, it should probably be recalled that ^{18}F-NaF is not immune to the display of therapy-induced flare phenomenon [195].

The final adoption of ^{18}F-NaF in replacing standard bone scintigraphy will likely depend on the cost and availability issues in a balancing act with the established increased diagnostic performance. The current emphasis on comparative effectiveness research may be able to provide valuable information for clinical decision making in individual patients and as a matter of health care policy in more general terms.

Prostate-Specific Membrane Antigen (PSMA)

PSMA is a cell surface transmembrane glycoprotein that is overexpressed on prostate tumor cells and thus provides a rational target not only for diagnosis and direct therapy but also for monitoring of PSMA expression changes with non–PSMA-based therapy [196]. For example, it has been reported that PSMA expression may be suppressed by androgen treatment, whereas antiandrogens (e.g., MDV3100) may up-regulate its expression [197].

Despite the relevance of PSMA in prostate cancer, the currently available ^{111}In-labeled capromab pendetide, which targets the internal moiety of PSMA in apoptotic or necrotic tissue, has shown limited predictive value in imaging the prostate fossa and has low sensitivity for detecting osseous metastases [198]. The PET radiotracer 89Zr-desferrioxamine B (DFO)-7E11 (half-life, 78.4 hours), which also targets the intracellular epitope of PSMA in dead or dying cells, has been recently evaluated in murine xenograft models of human prostate cancer and showed potential utility for monitoring and quantifying tumor response to irradiation [199].

There have also been significant efforts in designing other tracers that target PSMA [200–203]. J591 is a monoclonal antibody against the extracellular domain of PSMA that has been radiolabeled with 89Zr-desferrioxamine B (DFO)-7E11 for immunoPET of PSMA expression in live (as opposed to dying or dead) prostate cancer cells [204]. Other platforms include the use of PSMA inhibitors, such as ^{18}F-labeled *N*-[N-[(S)-1,3-Dicarboxypropyl] carbamoyl]-4-[^{18}F]fluorobenzyl-l-cysteine and ^{18}F-labeled phosphoramidate peptidomimetic, which have been shown in preclinical animal model studies to localize to PSMA-positive–expressing tumors with high specificity [205, 206].

Gene-Mediated Imaging

Interesting research is being performed in gene-mediated theranostics to diagnose and treat castration-resistant prostate cancer [207–210]. These methods include the potential utility of a fused enhancer derived from the PSA and the PSMA gene regulatory region with activity augmentation by the two-step transcriptional amplification system [211–213]. The augmented prostate-specific two-step transcriptional amplification method has also been shown to be AR dependent, which can potentially reflect the functional status of AR [214]. In one experiment, recombinant human adenoviral vectors were used to directly image nodal metastases of a prostate cancer model through prostate-restricted tumor expression of optical and PET reporter genes [215]. Such a platform may allow direct noninvasive visualization and characterization of the sentinel lymph node, such as the reporter gene herpes simplex virus type 1 TK and reporter probe 9-(4-(^{18}F) Fluoro-3-[hydroxymethyl]butyl)guanine, instead of the current indirect method with sentinel lymph node localization followed by tissue sampling. Such a platform will also allow the possibility of tumor-specific suicide gene therapy with prodrugs such as ganciclovir [216, 217]. These encouraging results will be complemented by additional studies on cancer specificity versus tissue specificity, efficiency of reporter gene delivery, transduction, and host immunoreactivity.

Summary

There has been much recent activity in the research and development of PET radiotracers for potential use in prostate cancer. Many of these radiotracers are in the early phases of evaluation in preclinical studies, whereas some are being tested in pilot clinical projects. The most common PET radiotracer, FDG, may have its major role in monitoring of treatment response in advanced metastatic prostate cancer. Although both ^{11}C-acetate and ^{11}C-choline appear to be somewhat equally useful in imaging prostate cancer in individual patients, most of the recent focus has been on ^{18}F-fluorocholine for detection of locally recurrent or metastatic disease in men with PSA relapse. Fluorine-18-NaF may soon replace standard ^{99m}Tc-based bone scintigraphy in view of its superior diagnostic performance. Other nonspecific radiotracers for prostate cancer, such as ^{18}F-FMAU, ^{18}F-anti-FACBC, and ^{68}Ga-AMBA, may provide new insights in prostate cancer biology that will also be useful in specific clinical circumstances. More specific radiotracers, such as ^{18}F-FDHT, PSMA, and gene-based bio-markers, may offer new ways to understand the biologic and functional heterogeneity of prostate cancer and to assess responses to the emerging targeted therapies. On the basis of the current evidence, the future routine clinical use of PET in the imaging evaluation of prostate cancer is ensured.

Acknowledgments

I thank Bhushan Desai for help with the preparation of Figures 1 and 5.

This work was funded by the National Institutes of Health, National Cancer Institute (grants R01-CA111613 and R21-CA142426).

References

1. Scher HI, Morris MJ, Basch E, Heller G. End points and outcomes in castrate-resistant prostate cancer: from clinical trials to clinical practice. J Clin Oncol. 2011; 29:3695–3704. [PubMed: 21859988]
2. Agarwal N, Sonpavde G, Sternberg CN. Novel molecular targets for the therapy of castration-resistant prostate cancer. Eur Urol. 2012; 61:950–960. [PubMed: 22209376]
3. Mease RC. Radionuclide based imaging of prostate cancer. Curr Top Med Chem. 2010; 10:1600–1616. [PubMed: 20583988]
4. Beheshti M, Langsteger W, Fogelman I. Prostate cancer: role of SPECT and PET in imaging bone metastases. Semin Nucl Med. 2009; 39:396–407. [PubMed: 19801219]
5. Hong H, Zhang Y, Sun J, Cai W. Positron emission tomography imaging of prostate cancer. Amino Acids. 2010; 39:11–27. [PubMed: 19946787]
6. Emonds KM, Swinnen JV, Mortelmans L, Mottaghy FM. Molecular imaging of prostate cancer. Methods. 2009; 48:193–199. [PubMed: 19362147]
7. Mottet N, Bellmunt J, Bolla M, et al. EAU guidelines on prostate cancer. Part II. Treatment of advanced, relapsing, and castration-resistant prostate cancer. Eur Urol. 2011; 59:572–583. [PubMed: 21315502]
8. Bouchelouche K, Capala J, Oehr P. Positron emission tomography/computed tomography and radioimmunotherapy of prostate cancer. Curr Opin Oncol. 2009; 21:469–474. [PubMed: 19535981]
9. Bouchelouche K, Tagawa ST, Goldsmith SJ, et al. PET/CT imaging and radioimmunotherapy of prostate cancer. Semin Nucl Med. 2011; 41:29–44. [PubMed: 21111858]
10. Karam JA, Mason RP, Koeneman KS, Antich PP, Benaim EA, Hsieh JT. Molecular imaging in prostate cancer. J Cell Biochem. 2003; 90:473–483. [PubMed: 14523981]
11. Apolo AB, Pandit-Taskar N, Morris MJ. Novel tracers and their development for the imaging of metastatic prostate cancer. J Nucl Med. 2008; 49:2031–2041. [PubMed: 18997047]
12. Sanz G, Rioja J, Zudaire J, Berián JM, Richter JA. PET and prostate cancer. World J Urol. 2004; 22:351–352. [PubMed: 15503049]

13. Huang CW, Li Z, Cai H, Chen K, Shahinian T, Conti PS. Design, synthesis and validation of inetgrin a2b1-targeted probe for microPET imaging of prostate cancer. Eur J Nucl Med Mol Imaging. 2011; 38:1313–1322. [PubMed: 21350963]
14. Zhang X, Xiong Z, Wu Y, et al. Quantitative PET imaging of tumor integrin alphavbeta3 expression with ^{18}F-FRGD2. J Nucl Med. 2006; 47:113–121. [PubMed: 16391195]
15. Lepin EJ, Leyton JV, Zhou Y, et al. An affinity matured minibody for PET imaging of prostate stem cell antigen (PSCA)-expressing tumors. Eur J Nucl Med Mol Imaging. 2010; 37:1529–1538. [PubMed: 20354850]
16. Leyton JV, Olafsen T, Sherman MA, et al. Engineered humanized diabodies for microPET imaging of prostate stem cell antigen expressing tumors. Protein Eng Des Sel. 2009; 22:209–216. [PubMed: 18957406]
17. Leyton JV, Olafsen T, Lepin EJ, et al. Humanized radioiodinated minibody for imaging of prostate stem cell antigen-expressing tumors. Clin Cancer Res. 2008; 14:7488–7496. [PubMed: 19010866]
18. Olafsen T, Gu Z, Sherman MA, et al. Targeting, imaging, and therapy using a humanized anti-prostate stem cell antigen (PSCA) antibody. J Immunother. 2007; 30:396–405. [PubMed: 17457214]
19. Vāvere AL, Lewis JS. Examining the relationship between Cu-ATSM hypoxia selectivity and fatty acid synthase expression in human prostate cancer cell lines. Nucl Med Biol. 2008; 35:273–279. [PubMed: 18355682]
20. Garcia-Parra R, Wood D, Shah RB, et al. Investigation on tumor hypoxia in resectable primary prostate cancer as demonstrated by ^{18}F-FAZA PET/CT utilizing multimodality fusion techniques. Eur J Nucl Med Mol Imaging. 2011; 38:1816–1823. [PubMed: 21833840]
21. Yapp DT, Woo J, Kartono A, et al. Non-invasive evaluation of tumor hypoxia in the Shionogi tumor model for prostate cancer with ^{18}F-EF5 and positron emission tomography. BJU Int. 2007; 99:1154–1160. [Erratum in *BJU Int* 2007; 99:1161]. [PubMed: 17309552]
22. Gillies RJ, Gatenby RA. Adaptive landscapes and emergent phenotypes: why do cancers have high glycolysis? J Bioenerg Biomembr. 2007; 39:251–257. [PubMed: 17624581]
23. Gillies RJ, Robey I, Gatenby RA. Causes and consequences of increased glucose metabolism of cancers. J Nucl Med. 2008; 49(suppl 2):24S–42S. [PubMed: 18523064]
24. Alavi A, Lakhani P, Mavi A, Kung JW, Zhuang H. PET: a revolution in medical imaging. Radiol Clin North Am. 2004; 42:983–1001. [PubMed: 15488553]
25. Macheda ML, Rogers S, Bets JD. Molecular and cellular regulation of glucose transport (GLUT) proteins in cancer. J Cell Physiol. 2005; 202:654–662. [PubMed: 15389572]
26. Smith TA. Mammalian hexokinases and their abnormal expression in cancer. Br J Biomed Sci. 2000; 57:170–178. [PubMed: 10912295]
27. Effert P, Beniers AJ, Tamimi Y, Handt S, Jakse G. Expression of glucose transporter 1 (GLUT-1) in cell lines and clinical specimen from human prostate adenocarcinoma. Anticancer Res. 2004; 24:3057–3063. [PubMed: 15517916]
28. Stewart GD, Gray K, Pennington CJ, et al. Analysis of hypoxia-associated gene expression in prostate cancer: lysyl oxidase and glucose transporter 1 expression correlate with Gleason score. Oncol Rep. 2008; 20:1561–1567. [PubMed: 19020742]
29. Reinicke K, Sotomayor P, Cisterna P, Delgado C, Nualart F, Godoy A. Cellular distribution of Glut-1 and Glut-5 in benign and malignant human prostate tissue. J Cell Biochem. 2012; 113:553–562. [PubMed: 21938742]
30. Jadvar H, Xiankui L, Shahinian A, et al. Glucose metabolism of human prostate cancer mouse xenografts. Mol Imaging. 2005; 4:91–97. [PubMed: 16105512]
31. Kukuk D, Reischl G, Raguin O, et al. Assessment of PET tracer uptake in hormone-independent and hormone-dependent xenograft prostate cancer mouse models. J Nucl Med. 2011; 52:1654–1663. [PubMed: 21859811]
32. Emonds KM, Swinnen JV, van Weerden WM, et al. Do androgens control the uptake of ^{18}F-FDG, ^{11}C-choline and ^{11}C-aceatte in human prostate cancer cell lines? Eur J Nucl Med Mol Imaging. 2011; 38:1842–1853. [PubMed: 21732108]
33. Jadvar H, Ye W, Groshen S, et al. [F-18]-fluorodeoxyglucose PET-CT of the normal prostate gland. Ann Nucl Med. 2008; 22:787–793. [PubMed: 19039557]

34. Salminen E, Hogg A, Binns D, et al. Investigations with FDG PET scanning in prostate cancer show limited value for clinical practice. Acta Oncol. 2002; 41:425–429. [PubMed: 12442917]
35. Shiiba M, Ishihara K, Kimura G, et al. Evaluation of primary cancer using (11C)-methionine-PET/CT and (18)F-FDG-PET/CT. Ann Nucl Med. 2011; 26:138–145. [PubMed: 22069194]
36. Minamimoto R, Uemura H, Sano F, et al. The potential of FDG PET/CT for detecting prostate cancer in patients with an elevated serum PSA level. Ann Nucl Med. 2011; 25:21–27. [PubMed: 20931305]
37. Han EJ, Ho J, Choi WH, Yoo IR, Chung SK. Significance of incidental focal uptake in prostate on 18-fluoro-2-deoxyglucose positron emission tomography CT images. Br J Radiol. 2010; 83:915–920. [PubMed: 20965901]
38. Oyama N, Akino H, Suzuki Y, et al. The increased accumulation of ^{18}F-fluorodeoxyglucose in untreated prostate cancer. Jpn J Clin Oncol. 1999; 29:623–629. [PubMed: 10721945]
39. Cookson MS, Aus G, Burnett AL, et al. Variation in the definition of biochemical recurrence in patients treated for localized prostate cancer: the American Urological Association Prostate Guidelines for Localized Prostate Cancer Update Panel report and recommendations for a standard in the reporting of surgical outcomes. J Urol. 2007; 177:540–545. [PubMed: 17222629]
40. Roach M 3rd, Hanks G, Thames H Jr, et al. Defining biochemical failure following radiotherapy with or without hormonal therapy in men with clinically localized prostate cancer: recommendations of the RTOG-ASTRO Phoenix Consensus Conference. Int J Radiat Oncol Biol Phys. 2006; 65:965–974. [PubMed: 16798415]
41. Schöder H, Hermann K, Gönen M, et al. 2-^{18}F-fluorodeoxyglucose positron emission tomography for detection of disease in patients with prostate-specific antigen relapse after radical prostatectomy. Clin Cancer Res. 2005; 11:4761–4769. [PubMed: 16000572]
42. Chang CH, Wu HU, Tsai JJ, et al. Detecting metastatic pelvic lymph nodes by ^{18}F-2-deoxyglucose positron emission tomography in patients with prostate specific antigen relapse after treatment for localized prostate cancer. Urol Int. 2003; 70:311–315. [PubMed: 12740497]
43. Jadvar H, Desai B, Ji L, et al. Prospective evaluation of ^{18}F-NaF and ^{18}F-FDG PET/CT in detection of occult metastatic disease in biochemical recurrence of prostate cancer. Clin Nucl Med. (in press).
44. Morris MJ, Akhurst T, Osman I, et al. Fluoridated deoxyglucose positron emission tomography imaging in progressive metastatic prostate cancer. Urology. 2002; 59:913–918. [PubMed: 12031380]
45. Jadvar H. Prostate cancer: PET with ^{18}F-FDG, ^{18}F- or ^{11}C-acetate, and ^{18}F- or ^{11}C-choline. J Nucl Med. 2011; 52:81–89. [PubMed: 21149473]
46. Jadvar H, Pinski J, Quinn D, et al. PET/CT with FDG in metastatic prostate cancer: castrate-sensitive vs. castrate-resistant disease. J Nucl Med. 2009; 50(suppl 2):460.
47. Fox J, Morris MJ, Larson SM, Schöder H, Scher HI. Developing imaging strategies for castration resistant prostate cancer. Acta Oncol. 2011; 50(suppl 1):39–48. [PubMed: 21604939]
48. Oyama N, Akino H, Suzuki Y, et al. FDG PET for evaluating the change of glucose metabolism in prostate cancer after androgen ablation. Nucl Med Commun. 2001; 22:963–969. [PubMed: 11505204]
49. Jadvar H, Desai B, Quinn D, et al. Treatment response assessment of metastatic prostate cancer with FDG PET/CT. J Nucl Med. 2011; 52(suppl 1):1908.
50. Jadvar, H.; Desai, B.; Ji, L., et al. Comparison of imaging- and PSA-based treatment response criteria in metastatic prostate cancer: a preliminary analysis. 97th RSNA scientific assembly and annual meeting; Oak Brook, IL: Radiological Society of North America; 2011.
51. Hillner BE, Siegel BA, Shields AF, et al. Relationship between cancer type and impact of PET and PET/CT on intended management: findings of the National Oncologic PET Registry. J Nucl Med. 2008; 49:1928–1935. [PubMed: 18997054]
52. Oyama N, Akino H, Suzuki Y, et al. Prognostic value of 2-deoxy-2-[F-18]fluoro-D-glucose positron emission tomography imaging for patients with prostate cancer. Mol Imaging Biol. 2002; 4:99–104. [PubMed: 14538053]
53. Meirelles GS, Schoder H, Ravizzini GC, et al. Prognostic value of baseline [^{18}F]fluorodeoxyglucose positron emission tomography and ^{99m}Tc-MDP bone scan in

progressing metastatic prostate cancer. Clin Cancer Res. 2010; 16:6093–6099. [PubMed: 20975102]

54. Soloviev D, Fini A, Chierichetti F, et al. PET imaging with ^{11}C-acetate in prostate cancer: a biochemical, radiochemical, and clinical perspective. Eur J Nucl Med Mol Imaging. 2008; 35:942–949. [PubMed: 18338167]
55. Yoshimoto M, Waki A, Yonekura Y, et al. Characterization of acetate metabolism in tumor cells in relation to cell proliferation: acetate metabolism in tumor cells. Nucl Med Biol. 2001; 28:117–122. [PubMed: 11295421]
56. Liu Y. Fatty acid oxidation is a dominant bioenergetic pathway in prostate cancer. Prostate Cancer Prostatic Dis. 2006; 9:230–234. [PubMed: 16683009]
57. Vāvere AL, Kridel SJ, Wheeler FB, et al. 1-^{11}C-acetate as a PET radiopharmaceutical for imaging fatty acid synthase expression in prostate cancer. J Nucl Med. 2008; 49:327–334. [PubMed: 18199615]
58. Pflug BR, Pecher SM, Brink AW, et al. Increased fatty acid synthase expression and activity during progression of prostate cancer in the TRAMP model. Prostate. 2003; 57:245–254. [PubMed: 14518031]
59. Seltzer MA, Jahan SA, Sparks R, et al. Radiation dose estimates in humans for (11)C-acetate whole-body PET. J Nucl Med. 2004; 45:1233–1236. [PubMed: 15235071]
60. Schiepers C, Hoh CK, Nuyts J, et al. 1-^{11}C-acetate kinetics of prostate cancer. J Nucl Med. 2008; 49:206–215. [PubMed: 18199613]
61. Kato T, Tsukamoto E, Kuge Y, et al. Accumulation of [(11)C]acetate in normal prostate and benign prostatic hyperplasia: comparison with prostate cancer. Eur J Nucl Med Mol Imaging. 2002; 29:1492–1495. [PubMed: 12397469]
62. Oyama N, Akino H, Kanamaru H, et al. ^{11}C-acetate PET imaging of prostate cancer. J Nucl Med. 2002; 43:181–186. [PubMed: 11850482]
63. Yu EY, Muzi M, Hackenvracht JA. C11-aceatte and F-18 FDG PET for men with prostate cancer bone metastases: relative findings and response to therapy. Clin Nucl Med. 2011; 36:192–198. [PubMed: 21285676]
64. Kotzerke J, Volkmer BG, Neumaier B, et al. Carbon-11 acetate positron emission tomography can detect local recurrence of prostate cancer. Eur J Nucl Med Mol Imaging. 2002; 29:1380–1384. [PubMed: 12271422]
65. Sandblom G, Sorensen J, Lundin N, et al. Positron emission tomography with ^{11}C-acetate for tumor detection and localization in patients with prostate specific antigen relapse after radical prostatectomy. Urology. 2006; 67:996–1000. [PubMed: 16698359]
66. Oyama N, Miller TR, Dehdashti F, et al. ^{11}C-acetate PET imaging of prostate cancer: detection of recurrent disease at PSA relapse. J Nucl Med. 2003; 44:549–555. [PubMed: 12679398]
67. Matthies A, Ezziddin S, Ulrich EM, et al. Imaging of prostate cancer metastases with ^{18}F-fluoroacetate using PET/CT. Eur J Nucl Med Mol Imaging. 2004; 31:797. [PubMed: 14985862]
68. Ponde DE, Dence CS, Oyama N, et al. ^{18}F-fluoroacetate: a potential acetate analog for prostate tumors imaging—in vivo evaluation of ^{18}F-fluoroacetate versus ^{11}C-acetate. J Nucl Med. 2007; 48:420–428. [PubMed: 17332620]
69. Lindhe O, Sun A, Ulin J, Rahman O, Långström B, Sörensen J. [(18)F]Fluoroacetate is not a functional analogue of [(11)C]acetate in normal physiology. Eur J Nucl Med Mol Imaging. 2009; 36:1453–1459. [PubMed: 19387639]
70. Kotzerke J, Volkmer BG, Glatting G, et al. Intra-individual comparison of [^{11}C]acetate and [^{11}C]choline PET for detection of metastases of prostate cancer. Nuklearmedizin. 2003; 42:25–30. [PubMed: 12601451]
71. Janardhan S, Srivani P, Sastry GN. Choline kinase: an important target for cancer. Curr Med Chem. 2006; 13:1169–1186. [PubMed: 16719778]
72. Contractor K, Challapalli A, Barwick T, et al. Use of [^{11}C]choline PET-CT as a noninvasive method for detecting pelvic lymph node status from prostate cancer and relationship with choline kinase expression. Clin Cancer Res. 2011; 17:7673–7683. [PubMed: 22038995]

73. Hara T, Bansal A, DeGrado TR. Effect of hypoxia on the uptake of [methyl-^{3}H]choline, [1-^{14}C]acetate and [^{18}F]FDG in cultured prostate cancer cells. Nucl Med Biol. 2006; 33:977–984. [PubMed: 17127170]
74. Breeuwsma AJ, Pruim J, Jongen MM, et al. In vivo uptake of [^{11}C]choline does not correlate with cell proliferation in human prostate cancer. Eur J Nucl Med Mol Imaging. 2005; 32:668–673. [PubMed: 15765234]
75. Reischl G, Bieg C, Schmiedl O, Solbach C, Machulla HJ. Highly efficient automated synthesis of [(11)C]choline for multi dose utilization. Appl Radiat Isot. 2004; 60:835–838. [PubMed: 15110347]
76. Scher B, Seitz M, Albinger W, et al. Value of ^{11}C-choline PET and PET-CT in patients with suspected prostate cancer. Eur J Nucl Med Mol Imaging. 2007; 34:45–53. [PubMed: 16932935]
77. Farsad M, Schiavina R, Castellucci P, et al. Detection and localization of prostate cancer: correlation of (^{11}C)C-choline PET/CT with histopathologic step-section analysis. J Nucl Med. 2005; 46:1642–1649. [PubMed: 16204714]
78. Rinnab L, Blumstein NM, Mottaghy FM, et al. ^{11}C-choline positron emission tomography/computed tomography and transrectal ultrasonography for staging localized prostate cancer. BJU Int. 2007; 99:1421–1426. [PubMed: 17355373]
79. Martorana G, Schiavina R, Cort B, et al. ^{11}C-choline positron emission tomography/computed tomography for tumor localization of primary prostate cancer in comparison with 12-core biopsy. J Urol. 2006; 176:954–960. [PubMed: 16890665]
80. Souvatzoglou M, Weirich G, Schwarzenboeck S, et al. The sensitivity of [^{11}C]choline PET/CT to localize prostate cancer depends on the tumor configuration. Clin Cancer Res. 2011; 17:3751–3759. [PubMed: 21493868]
81. Giovacchini G, Picchio M, Coradesschi E, et al. ^{11}C-choline uptake with PET/CT for the initial diagnosis of prostate cancer: relation to PSA levels, tumor stage and anti-androgenic therapy. Eur J Nucl Med Mol Imaging. 2008; 35:1065–1073. [PubMed: 18200444]
82. Testa C, Schiavina R, Lodi R, et al. Prostate cancer: sextant localization with MR imaging, MR spectroscopy, and ^{11}C-choline PET-CT. Radiology. 2007; 244:797–806. [PubMed: 17652190]
83. Yamaguchi T, Lee J, Uemura H, et al. Prostate cancer: a comparative study of ^{11}C-choline PET and MR imaging combined with proton MR spectroscopy. Eur J Nucl Med Mol Imaging. 2005; 32:742–748. [PubMed: 16052370]
84. Eschmann SM, Pfannenberg AC, Rieger A, et al. Comparison of ^{11}C-choline PET-CT and whole body MRI for staging of prostate cancer. Nuklearmedizin. 2007; 46:161–168. [PubMed: 17938748]
85. Beer AJ, Eiber M, Souvatzoglou M, et al. Restricted water diffusibility as measured by diffusion-weighted MR imaging and choline uptake in (11)C-choline PET/CT are correlated in pelvic lymph nodes in patients with prostate cancer. Mol Imaging Biol. 2011; 13:352–361. [PubMed: 20490932]
86. Park H, Piert MR, Khan A, et al. Registration methodology for histological sections and in vivo imaging of human prostate. Acad Radiol. 2008; 15:1027–1039. [PubMed: 18620123]
87. Murphy RC, Kawashima A, Peller PJ. The utility of ^{11}C-choline PET/CT for imaging prostate cancer: a pictorial guide. AJR. 2011; 196:1390–1398. [PubMed: 21606304]
88. Picchio M, Crivellaro C, Giovacchini G, et al. PET-CT for treatment planning in prostate cancer. Q J Nucl Med Mol Imaging. 2009; 53:245–268. [PubMed: 19293771]
89. Picchio M, Briganti A, Fanti S, et al. The role of choline positron emission tomography/computed tomography in the management of patients with prostate-specific antigen progression after radical treatment of prostate cancer. Eur Urol. 2011; 59:51–60. [PubMed: 20869161]
90. Krause BJ, Souvatzpglou M, Tuncel M, et al. The detection rate of [(11)C]choline-PET/CT depends on the serum PSA-value in patients with biochemical recurrence of prostate cancer. Eur J Nucl Med Mol Imaging. 2008; 35:18–23. [PubMed: 17891394]
91. Kotzerke J, Prang J, Neumaier B, et al. Experience with carbon-11 choline positron emission tomography in prostate carcinoma. Eur J Nucl Med. 2000; 27:1415–1419. [PubMed: 11007527]
92. Rinnab L, Mottaghy FM, Blumstein NM, et al. Evaluation of [^{11}C]choline positron emission tomography in patients with increasing prostate-specific antigen levels after primary treatment for prostate cancer. BJU Int. 2007; 100:786–793. [PubMed: 17822459]

93. de Jong IJ, Pruim J, Elsinqa PH, Vaalburg W, Mensink HJ. ^{11}C-choline positron emission tomography for the evaluation after treatment of localized prostate cancer. Eur Urol. 2003; 44:32–38. [PubMed: 12814672]

94. Reske SN, Blumstein NM, Glatting G. [(^{11}C)] choline PET/CT imaging in occult local relapse of prostate cancer after radical prostatectomy. Eur J Nucl Med Mol Imaging. 2008; 35:9–17. [PubMed: 17828534]

95. Scattoni V, Picchio M, Suardi N, et al. Detection of lymph-node metastases with integrated [^{11}C] choline PET/CT in patients with PSA failure after radical retropubic prostatectomy: results confirmed by open pelvic-retroperitoneal lymphadenectomy. Eur Urol. 2007; 52:423–429. [PubMed: 17397992]

96. Castellucci P, Fuccio C, Nanni C, et al. Influence of trigger PSA and PSA kinetics on ^{11}C-choline PET/CT detection rate in patients with biochemical relapse after radical prostatectomy. J Nucl Med. 2009; 50:1394–1400. [PubMed: 19690023]

97. Richter JA, Rodríguez M, Rioja J, et al. Dual tracer ^{11}C-choline and FDG-PET in the diagnosis of biochemical prostate cancer relapse after radical treatment. Mol Imaging Biol. 2010; 12:210–217. [PubMed: 19543774]

98. Picchio M, Spinapolice EG, Fallanca F, et al. [^{11}C]choline PET/CT detection of bone metastases in patients with PSA progression after primary treatment for prostate cancer: comparison with bone scintigraphy. Eur J Nucl Med Mol Imaging. 2012; 39:13–26. [PubMed: 21932120]

99. Fuccio C, Schiavina R, Castellucci P, et al. Androgen deprivation therapy influences the uptake of ^{11}C-choline in patients with recurrent prostate cancer: the preliminary results of a sequential PET/CT study. Eur J Nucl Med Mol Imaging. 2011; 38:1985–1989. [PubMed: 21732105]

100. DeGrado TR, Coleman RE, Wang S, et al. Synthesis and evaluation of ^{18}F-labeled choline as an oncologic tracer for positron emission tomography: initial findings in prostate cancer. Cancer Res. 2001; 61:110–117. [PubMed: 11196147]

101. Bauman G, Belhocine T, Kovacs M, Ward A, Beheshti M, Rachinsky I. (^{18}F)F-fluorocholine for prostate cancer imaging: a systematic review of literature. Prostate Cancer Prostatic Dis. 2012; 15:45–55. [PubMed: 21844889]

102. Price DT, Coleman RE, Liao RP, et al. Comparison of [18 F]fluorocholine and [18 F]fluorodeoxyglucose for positron emission tomography of androgen dependent and androgen independent prostate cancer. J Urol. 2002; 168:273–280. [PubMed: 12050555]

103. Jadvar H, Gurbuz A, Li X, et al. Choline autoradiography of human prostate cancer xenograft: effect of castration. Mol Imaging. 2008; 7:147–152. [PubMed: 19123985]

104. Igerc I, Kohlfürst S, Gallowitsch HJ, et al. The value of ^{18}F-choline PET/CT in patients with elevated PSA-level and negative prostate needle biopsy for localization of prostate cancer. Eur J Nucl Med Mol Imaging. 2008; 35:976–983. [PubMed: 18188560]

105. Kwee SA, Coel MN, Lim J, Ko JP. Prostate cancer localization with 18fluorine fluorocholine positron emission tomography. J Urol. 2005; 173:252–255. [PubMed: 15592091]

106. Beheshti M, Imamovic L, Broinger G, et al. ^{18}F choline PET/CT in the preoperative staging of prostate cancer in patients with intermediate or high risk of extracapsular disease: a prospective study of 130 patients. Radiology. 2010; 254:925–933. [PubMed: 20177103]

107. Pelosi E, Arena V, Skanjeti A, et al. Role of whole-body (^{18}F)-choline PET/CT in disease detection in patients with biochemical relapse after radical treatment for prostate cancer. Radiol Med (Torino). 2008; 113:895–904. [PubMed: 18414809]

108. Heinisch M, Dirisamer A, Loidl W, et al. Positron emission tomography/computed tomography with F-18 fluorocholine for restaging of prostate cancer patients: meaningful at PSA < 5 ng/mL? Mol Imaging Biol. 2006; 8:43–48. [PubMed: 16315004]

109. Graute V, Jansen N, Ubeleis C, et al. Relationship between PSA kinetics and ^{18}F-fluorolcholine PET/CT detection rates of recurrence in patients with prostate cancer after total prostatectomy. Eur J Nucl Med Mol Imaging. 2012; 39:271–282. [PubMed: 22086143]

110. Schillaci O, Calabria F, Tavolozza M, et al. Influence of PSA, PSA velocity, and PSA doubling time on contrast-enhanced (18)F-choline PET/CT detection rate in patients with rising PSA after radical prostatectomy. Eur J Nucl Med Mol Imaging. 2012; 39:589–596. [PubMed: 22231016]

111. Langsteger W, Balogova S, Huchet V, et al. Fluorocholine (^{18}F) and sodium fluoride (^{18}F) PET/CT in the detection of prostate cancer: prospective comparison of diagnostic performance determined by masked reading. Q J Nucl Med Mol Imaging. 2011; 55:448–457. [PubMed: 21738117]

112. Beheshti M, Vali R, Waldenberger P, et al. Detection of bone metastases in patients with prostate cancer by ^{18}F fluorocholine and ^{18}F fluoride PET-CT: a comparative study. Eur J Nucl Med Mol Imaging. 2008; 35:1766–1774. [PubMed: 18465129]

113. Beheshti M, Vali R, Waldenberger P, et al. The use of F-18 choline PET in the assessment of bone metastases in prostate cancer: correlation with morphological changes on CT. Mol Imaging Biol. 2009; 11:446–454. [PubMed: 19326171]

114. Jadvar H. Molecular imaging of prostate cancer with ^{18}F-fluorodeoxyglucose PET. Nat Rev Urol. 2009; 6:317–323. [PubMed: 19434102]

115. Mankoff DA, Shields AF, Krohn KA. PET imaging of cellular proliferation. Radiol Clin North Am. 2005; 43:153–167. [PubMed: 15693654]

116. Couturier O, Leost F, Campone M, et al. Is 3′-deoxy-3′-[^{18}F]fluorothymidine ([^{18}F]-FLT) the next tracer for routine clinical PET after [^{18}F]-FDG? Bull Cancer. 2005; 92:789–798. [PubMed: 16203269]

117. Nimmagadda S, Shields AF. The role of DNA synthesis imaging in cancer in the era of targeted therapeutics. Cancer Metastasis Rev. 2008; 27:575–587. [PubMed: 18512023]

118. Bading JR, Shields AF. Imaging of cell proliferation: status and prospects. J Nucl Med. 2008; 49(suppl 2):64S–80S. [PubMed: 18523066]

119. Shields AF, Mankoff DA, Graham MM, et al. Analysis of 2-carbon-11-thymidine blood metabolites in PET imaging. J Nucl Med. 1996; 37:290–296. [PubMed: 8667064]

120. Shields AF, Mankoff DA, Link JM, et al. [^{11}C] Thymidine and FDG to measure therapy response. J Nucl Med. 1998; 39:1757–1762. [PubMed: 9776283]

121. Mankoff DA, Shield AF, Graham MM, Link JM, Eary JF, Krohn KA. Kinetic analysis of 2-[carbon-11]thymidine PET imaging studies: compartmental model and mathematical analysis. J Nucl Med. 1998; 39:1043–1055. [PubMed: 9627342]

122. Mankoff DA, Shields AF, Link JM, et al. Kinetic analysis of 2-[^{11}C]thymidine PET imaging studies: validation studies. J Nucl Med. 1999; 40:614–624. [PubMed: 10210220]

123. Shields AF, Grierson JR, Dohmen BM, et al. Imaging proliferation in vivo with [F-18]FLT and positron emission tomography. Nat Med. 1998; 4:1334–1336. [PubMed: 9809561]

124. Grierson JR, Shields AF. Radiosynthesis of 3′-deoxy-3′-[(^{18}F]fluorothymidine: [(^{18}F)F]FLT for imaging of cellular proliferation in vivo. Nucl Med Biol. 2000; 27:143–156. [PubMed: 10773543]

125. Shields AF, Grierson JR, Muzik O, et al. Kinetics of 3′-deoxy-3′-[F-18]fluorothymidine uptake and retention in dogs. Mol Imaging Biol. 2002; 4:83–89. [PubMed: 14538051]

126. Oyama N, Ponde D, Dence C, Kim J, Tai YC, Welch MJ. Monitoring of therapy in androgen-dependent prostate tumor model by measuring tumor proliferation. J Nucl Med. 2004; 45:519–525. [PubMed: 15001697]

127. Oyama N, Hasegawa Y, Kiyono Y, et al. Early response assessment in prostate carcinoma by ^{18}F-fluorothymidine following anticancer therapy with docetaxel using preclinical tumor models. Eur J Nucl Med Mol Imaging. 2011; 38:81–89. [PubMed: 20878403]

128. Tehrani OS, Douglas KA, Lawhorn-Crews JM, Shields AF. Tracking cellular stress with labeled FMAU reflects changes in mitochondrial TK2. Eur J Nucl Med Mol Imaging. 2008; 35:1480–1488. [PubMed: 18265975]

129. Fanucchi MP, Leyland-Jones R, Young CW, et al. Phase I trial of 1-(2′-deoxy-2′-fluoro-1-beta-D-arabinofuranosyl)-5-methyluracil (FMAU). Cancer Treat Rep. 1985; 69:55–59. [PubMed: 2981621]

130. Conti PS, Alauddin MM, Fissekis JR, Schmall B, Watanabe KA. Synthesis of 2′-fluoro-5-[^{11}C]-methyl-1-beta-D-arabinofurasyluracil ([^{11}C]-FMAU): a potential nucleoside analog for in vivo study of cellular proliferation with PET. Nucl Med Biol. 1995; 22:783–789. [PubMed: 8535339]

131. Bading JR, Shahinian AH, Bathija P, Conti PS. Pharmacokinetics of the thymidine analog 2′-fluoro-5-[(14)C]-methyl-1-beat-D-arabinofuranosyluracil ([(14)C]FMAU in rat prostate tumor cell. Nucl Med Biol. 2000; 27:361–368. [PubMed: 10938471]

132. Wang H, Oliver P, Nan L, et al. Radiolabeled 2′-fluorodeoxyuracil-beat-D-arabinofuranoside (FAU) and 2′-fluoro-5-methyldeoxyuracil-beta-D-arabinofuranoside (FMAU) as tumor imaging agents in mice. Cancer Chemother Pharmacol. 2002; 49:419–424. [PubMed: 11976837]

133. Tehrani OS, Muzik O, Heilbrun LK, et al. Tumor imaging using 1-(2′-deoxy-^{18}F-fluoro-beta-D-arabinofuranosyl)thymine and PET. J Nucl Med. 2007; 48:1436–1441. [PubMed: 17785728]

134. Mangner TJ, Klecker RW, Anderson L, Shields AF. Synthesis of 2′-deoxy-2′-[^{18}F]fluoro-beta-D-arabinofuranosyl nucleosides, [^{18}F]FAU, [^{18}F] FMAU, [^{18}F]FBAU and [^{18}F]FIAU, as potential PET agents for imaging cellular proliferation: synthesis of [^{18}F] labeled FAU, FMAU, FBAU, FIAU. Nucl Med Biol. 2003; 30:215–224. [PubMed: 12745012]

135. de Vries EF, van Waarde A, Harmsen MC, et al. [(11)C]FMAU and [(18)F]FHPG as PET tracers for herpes simplex virus thymidine kinase activity and human cytomegalovirus infections. Nucl Med Biol. 2000; 27:113–119. [PubMed: 10773539]

136. Alauddin MM, Shahinian A, Gordon EM, Conti PS. Evaluation of 2′-deoxy-2′-fluoro-5-methyl-1-beta-D-arabinofurasyluracil as a potential gene imaging agent for HSV-tk expression in vivo. Mol Imaging. 2002; 1:74–81. [PubMed: 12920847]

137. Alauddin MM, Shahinian A, Park R, Tohme M, Fissekis JD, Conti PS. Synthesis and evaluation of 2′-deoxy-2′-^{18}F-fluoro-5-fluoro-1-beta-D-arabinofuranosyluracil as a potential PET imaging agent for suicide gene expression. J Nucl Med. 2004; 45:2063–2069. [PubMed: 15585483]

138. Kang KW, Min JJ, Chen X, Gambhir SS. Comparison of [^{14}C]FMAU, [^{3}H]FEAU, [^{14}C]FIAU, and [^{3}H]PCV for monitoring reporter gene expression of wild type and mutant herpes simplex virus type I thymidine kinase in cell culture. Mol Imaging Biol. 2005; 7:296–303. [PubMed: 16041591]

139. Li Z, Cai H, Conti PS. Automated synthesis of 2′-deoxy-2′-[^{18}F]fluoro-5-methyl-1-b-D-arabino-furanosyluracil ([^{18}F]-FMAU) using a one reactor radiosynthesis module. Nucl Med Biol. 2011; 38:201–206. [PubMed: 21315275]

140. Bading JR, Shahinian AH, Vail A, et al. Pharmacokinetics of the thymidine analog 2′-fluoro-5-methyl-1-beta-D-arabinofuranosyluracil (FMAU) in tumor-bearing rats. Nucl Med Biol. 2004; 31:407–418. [PubMed: 15093810]

141. Conti PS, Bading JR, Mouton PP, et al. In vivo measurement of cell proliferation in canine brain tumor using C-11-labeled FMAU and PET. Nucl Med Biol. 2008; 35:131–141. [PubMed: 18158952]

142. Nishii R, Volgia AY, Mawlawi O, et al. Evaluation of 2′-deoxy-2′-[(18)F]fluoro-5-methyl-1-beta-L:-arabinofuranosyluracil ([(18)F]-L:-FMAU) as a PET imaging agent for cellular proliferation: comparison with [(18)F]-D:-FMAU and [(18)F]FLT. Eur J Nucl Med Mol Imaging. 2008; 35:990–998. [PubMed: 18057932]

143. Sun H, Mangner TJ, Collins JM, et al. Imaging DNA synthesis in vivo with ^{18}F-FMAU and PET. J Nucl Med. 2005; 46:292–296. [PubMed: 15695789]

144. Shields AF. Positron emission tomography measurement of tumor metabolism and growth: its expanding role in oncology. Mol Imaging Biol. 2006; 8:141–150. [PubMed: 16534552]

145. Doeg KA, Polomski LL, Doeg LH. Androgen control of mitochondrial and nuclear DNA synthesis in male sex accessory tissue of castrate rats. Endocrinology. 1972; 90:1633–1638. [PubMed: 5020313]

146. Jadvar H, Yap L-I, Park R, et al. [^{18}F]-2′-fluoro-5-methyl-1-beta-D-arabinofuranosyluracil (^{18}F-FMAU) in prostate cancer: initial preclinical observations. Mol Imaging. (in press).

147. Sun H, Sloan A, Mangner TJ, et al. Imaging DNA synthesis with [^{18}F]FMAU and positron emission tomography in patients with cancer. Eur J Nucl Med Mol Imaging. 2005; 32:15–22. [PubMed: 15586282]

148. Alauddin MM, Shahinian A, Gordon EM, Conti PS. Direct comparison of radiolabeled probes FMAU, FHBG, and FHPG as PET imaging agents for HSV1-tk expression in a human breast cancer model. Mol Imaging. 2004; 3:76–84. [PubMed: 15296672]

149. Cai H, Li Z, Conti PS. The improved syntheses of 5-substituited 2′-[^{18}F]fluoro-2′-deoxy-arabinofuranosyluracil derivatives ([^{18}F]FAU, [^{18}F]FEAU, [^{18}F]FFAU, [^{18}F]FCAU, [^{18}F]FBAU and [^{18}F]FIAU) using a multistep one-pot strategy. Nucl Med Biol. 2011; 38:659–666. [PubMed: 21718941]
150. Trapman J, Brinkmann AO. The androgen receptor in prostate cancer. Pathol Res Pract. 1996; 192:752–760. [PubMed: 8880876]
151. Culig Z, Hobisch A, Hittmair A, et al. Androgen receptor gene mutations in prostate cancer. Implications for disease progression and therapy. Drugs Aging. 1997; 10:50–58. [PubMed: 9111707]
152. Jenster G. The role of the androgen receptor in the development and progression of prostate cancer. Semin Oncol. 1999; 26:407–421. [PubMed: 10482183]
153. Scher HI, Beer TM, Higano CS, et al. Antitumor activity of MDV3100 in castration-resistant prostate cancer: a phase 1–2 study. Lancet. 2010; 375:1437–1446. [PubMed: 20398925]
154. Morris M, Huang D, Kelly W, et al. Phase 1 trial of high-dose exogenous testosterone in patients with castration-resistant metastatic prostate cancer. Eur Urol. 2009; 56:237–244. [PubMed: 19375217]
155. Liu A, Dence CS, Welch MJ, Katzenellenbogen JA. Fluorine-18-labeled androgens: radiochemical synthesis and tissue distribution studies on six fluorine-substituted androgens, potential imaging agents for prostate cancer. J Nucl Med. 1992; 33:724–734. [PubMed: 1569482]
156. Parent EE, Dence CS, Sharp TL, Welch MJ, Katzenellenbogen JA. Synthesis and biological evaluation of a fluorine-18-labeled nonsteroidal androgen receptor antagonist, N-(3-[^{18}F]fluoro-4-nitronaphthyl)-cis-5-norobornene-endo-2,3-dicarboxylic imide. Nucl Med Biol. 2006; 33:615–624. [PubMed: 16843836]
157. Parent EE, Carlson KE, Katzenellenbogen JA. Synthesis of 7alpha-(fluormethyl)dihydrotetosterone and 7alpha-(fluoromethyl)nortestosteerone, structurally paired androgens designed to probe the role of sex hormone binding in imaging androgen receptors in prostate tumors by emission tomography. J Org Chem. 2007; 72:5546–5554. [PubMed: 17585812]
158. Larson SM, Morris M, Gunther I, et al. Tumor localization of 16beta-^{18}F-fluoro-5alpha-dihydrotestosterone versus ^{18}F-FDG in patients with progressive, metastatic prostate cancer. J Nucl Med. 2004; 45:366–373. [PubMed: 15001675]
159. Dehdashti F, Picus J, Michalski J, et al. Positron tomographic assessment of androgen receptors in prostatic carcinoma. Eur J Nucl Med Mol Imaging. 2005; 32:344–350. [PubMed: 15726353]
160. Beattie BJ, Smith-Jones PM, Jhanwar YS, et al. Pharmacokinetic assessment of the uptake of 16beta-^{18}F-fluoro-5alpha-dihydrotestosterine (FDHT) in prostate tumors as measured by PET. J Nucl Med. 2010; 51:183–192. [PubMed: 20080885]
161. Fox J, Blanc E, Schoder H, et al. Diversity of biology in castrate resistant prostate cancer. J Nucl Med. 2009; 50(suppl 2):523.
162. Zanzonico PB, Finn R, Pentlow KS, et al. PET-based radiation dosimetry in man of ^{18}F-fluorodihydrotestosterone, a new radiotracer for imaging prostate cancer. J Nucl Med. 2004; 45:1966–1971. [PubMed: 15534070]
163. Yang YS, Zhang X, Xiong Z, Chen X. Comparative in vitro and in vivo evaluation of two ^{64}Cu-labaled bombesin analogs in a mouse model of human prostate cancer. Nucl Med Biol. 2006; 33:371–380. [PubMed: 16631086]
164. Chen X, Park R, Hou Y, et al. MicroPET and autoradiographic imaging of GRP receptor expression with ^{64}Cu-DOTA-[Lys3]bombesin in human prostate adenocarcinoma xenografts. J Nucl Med. 2004; 45:1390–1397. [PubMed: 15299066]
165. Yang M, Gao H, Zhou Y, et al. F-labeled GRPR agonists and antagonists: a comparative study in prostate cancer imaging. Theranostics. 2011; 1:220–229. [PubMed: 21544226]
166. Lears KA, Ferdani R, Liang K, et al. In vitro and in vivo evaluation of ^{64}Cu-labeled SarAr-bombesin analogs in gastrin-releasing peptide receptor-expressing prostate cancer. J Nucl Med. 2011; 52:470–477. [PubMed: 21321264]

167. Honer M, Mu L, Stelfeld T, et al. ^{18}F-labeled bombesin analog for specific and effective targeting of prostate tumors expressing gastrin-releasing peptide receptors. J Nucl Med. 2011; 52:270–278. [PubMed: 21233180]

168. Lane SR, Nanda P, Rold TL, et al. Optimization, biological evaluation and microPET imaging of copper-64-labeled bombesin agonists, [^{64}Cu-NO2A-(X)-BBN(7-14)NH2], in a prostate tumor xenografted mouse model. Nucl Med Biol. 2010; 37:751–761. [PubMed: 20870150]

169. Ananias HJ, de Jong IJ, Diercks RA, van de Wiele C, Helfrich W, Elsinga PH. Nuclear imaging of prostate cancer with gastrin-releasing receptor targeted radiopharmaceuticals. Curr Pharm Des. 2008; 14:3033–3047. [PubMed: 18991717]

170. Garrison JC, Rold TL, Sieckman GL, et al. In vivo evaluation and small animal PET/CT of a prostate cancer mouse model using ^{64}Cu-bombesin analogs: side-by-side comparison of the CB-TE2A and DOTA chelation systems. J Nucl Med. 2007; 48:1327–1337. [PubMed: 17631556]

171. Zhang X, Cai W, Cao F, et al. ^{18}F-labeled bombe-sin analogs for targeting GRP receptor-expressing prostate cancer. J Nucl Med. 2006; 47:492–501. [PubMed: 16513619]

172. Rogers BE, Bigott HM, McCarthy DW, et al. MicroPET imaging of a gastrin-releasing peptide receptor-positive tumor in a mouse model of human prostate cancer using a ^{64}Cu-labeled bombe-sin analog. Bioconjug Chem. 2003; 14:756–763. [PubMed: 12862428]

173. Craft JM, De Silva RA, Lears KA, et al. In vitro and in vivo evaluation of a (64)Cu-labeled NO-TA-Bn-SCN-Aoc-bombesin analogue in gastrin-releasing peptide receptor expressing prostate cancer. Nucl Med Biol. 2012 [Epub ahead of print].

174. Schroeder RP, van Weerden WM, Krenning EP, et al. Gastrin-releasing receptor-based targeting using bombesin analogs is superior to metabolism-based targeting using choline for in vivo imaging of human prostate cancer xenografts. Eur J Nucl Med Mol Imaging. 2011; 38:1257–1266. [PubMed: 21431398]

175. Macapinlac HA, Humm JL, Akhurst T, et al. Differential metabolism and pharmacokinetics of L-[1-(11)C]-methionine and 2-[(^{18}F)F]fluoro-2-deoxy-D-glucose (FDG) in androgen independent prostate cancer. Clin Positron Imaging. 1999; 2:173–181. [PubMed: 14516541]

176. Nuñez R, Macapinlac HA, Yeung HW, et al. Combined ^{18}F-FDG and ^{11}C-methionine PET scans in pati8ents with newly progressive meta-static prostate cancer. J Nucl Med. 2002; 43:46–55. [PubMed: 11801702]

177. Tóth G, Lengyel Z, Balkay L, Salah MA, Trón L, Tóth C. Detection of prostate cancer with ^{11}C-methionine positron emission tomography. J Urol. 2005; 173:66–69. [PubMed: 15592030]

178. Oka S, Hattori R, Kurosaki F, et al. A preliminary study of anti-1-amino-3-^{18}F-fluorocyclobutyl-1-carboxylic acid for the detection of prostate cancer. J Nucl Med. 2007; 48:46–55. [PubMed: 17204698]

179. Oka S, Okudaira H, Yoshida Y, Schuster DM, Goodman MM, Shirakami Y. Transport mechanisms of *trans*-1-amino-3-fluoro[1-(^{14}C)cyclobutanecarboxylic acid in prostate cancer. Nucl Med Biol. 2012; 39:109–119. [PubMed: 21958853]

180. Okudaira H, Shikano N, Nishii R, et al. Putative transport mechanism and intracellular fate of *trans*-1-amino-3-^{18}F-fluorocyclobutanecarboxylic acid in human prostate cancer. J Nucl Med. 2011; 52:822–829. [PubMed: 21536930]

181. Schuster DM, Votaw JR, Nieh PT, et al. Initial experience with the radiotracer anti-1-amino-3-^{18}F-fluorocyclobutane-1-carboxylic acid with PET/CT in prostate carcinoma. J Nucl Med. 2007; 48:56–63. [PubMed: 17204699]

182. Schuster DM, Savir-Baruch B, Nieh PT, et al. Detection of recurrent prostate carcinoma with anti-1-amino-3-^{18}F-fluorocyclobutane-1-carboxylic acid PET/CT and ^{111}In-capromab pendetide SPECT/CT. Radiology. 2011; 259:852–861. [PubMed: 21493787]

183. Jani AB, Fox TH, Whitaker D, Schuster DM. Case study of anti-1-amino-3-^{18}F-fluorocyclobutane-1-carboxylic acid (anti-[F-18]FACBC) to guide prostate cancer radiotherapy target design. Clin Nucl Med. 2009; 34:279–284. [PubMed: 19387202]

184. Tombal B, Lecouvet F. Modern detection of prostate cancer's bone metastasis: is the bone scan era over? Adv Urol. 2012; 2012:893193. [PubMed: 22013439]

185. Shirrmeister H, Guhlmann A, Elsner K, et al. Sensitivity in detecting osseous lesions depends on anatomic localization: planar bone scintigraphy versus ^{18}F PET. J Nucl Med. 1999; 40:1623–1629. [PubMed: 10520701]

186. Grant FD, Fahey FH, Packard AB, Davis RT, Alavi A, Treves ST. Skeletal PET with ^{18}F-fluoride: applying new technology to an old tracer. J Nucl Med. 2008; 49:68–78. [PubMed: 18077529]

187. Czernin J, Satyamurthy N, Schiepers C. Molecular mechanisms of bone ^{18}F-NaF deposition. J Nucl Med. 2010; 51:1826–1829. [PubMed: 21078790]

188. Even-Sapir E, Mishani E, Flusser G, et al. ^{18}F-fluoride positron emission tomography and positron emission tomography/computed tomography. Semin Nucl Med. 2007; 37:462–469. [PubMed: 17920353]

189. Li Y, Tafti BA, Shaba W, Berenji GR. Superscan pattern of F-18 sodium fluoride PET/CT study in a case of prostate cancer. Clin Nucl Med. 2011; 36:1046–1048. [PubMed: 21975402]

190. Segall G, Delbeke D, Stabin MG, et al. SNM practice guideline for sodium ^{18}F-fluoride PET/CT bone scans 1. 0. J Nucl Med. 2010; 51:1813–1820. [PubMed: 21051652]

191. Hsu WK, Virk MS, Feeley BT, et al. Characterization of osteolytic, osteobalstic, and mixed lesions in a prostate cancer mouse model using ^{18}F-FDG and ^{18}F-fluoride PET/CT. J Nucl Med. 2008; 49:414–421. [PubMed: 18287261]

192. Kawaguchi M, Tateischi U, Shizukuishi K, Suzuki A, Inoue T. ^{18}F-fluoride uptake in bone metastasis: morphologic and metabolic analysis on integrated PET/CT. Ann Nucl Med. 2010; 24:241–247. [PubMed: 20333485]

193. Even-Sapir E, Metser U, Mishani E, Lievshitz G, Lerman H, Leibovitch I. The detection of bone metastases in patients with high-risk prostate cancer: ^{99m}Tc-MDP planar bone scintigraphy, single- and multi-field-of-view SPECT, ^{18}F-fluoride PET, and ^{18}F-fluoride PET/CT. J Nucl Med. 2006; 47:287–297. [PubMed: 16455635]

194. Cook GJ, Parker C, Chua S, Johnson B, Aksnes AK, Lewington VJ. ^{18}F-fluoriode: changes in uptake as a method to assess response in bone metastases from castrate-resistant prostate cancer patients treated with 223Ra-chloride (Alpha-radin). EJNMMI Res. 2011; 1:4. [PubMed: 22214491]

195. Wade AA, Scott JA, Kuter I, Fischman AJ. Flare response in ^{18}F-fluoride ion PET bone scanning. AJR. 2006; 186:1783–1786. [PubMed: 16714674]

196. Bouchelouche K, Choyke PL, Capala J. Prostate-specific membrane antigen: a target for imaging and therapy with radionuclides. Discov Med. 2010; 9:55–61. [PubMed: 20102687]

197. Evans MJ, Smith-Jones PM, Wongvipat J, et al. Noninvasive measurement of androgen receptor signaling with positron emitting radiopharmaceutical that targets prostate-specific membrane antigen. Proc Natl Acad Sci USA. 2011; 108:9578–9582. [PubMed: 21606347]

198. Haseman MK, Rosenthal SA, Polascik TJ. Capromab pendetide imaging of prostate cancer. Cancer Biother Radiopharm. 2000; 15:131–140. [PubMed: 10803318]

199. Ruggiero A, Holland JP, Hudolin T, et al. Targeting the internal epitope of prostate-specific membrane antigen with 89Zr-7E11 immunoPET. J Nucl Med. 2011; 52:1608–1615. [PubMed: 21908391]

200. Alt K, Wiehr S, Ehrlichmann W, et al. High-resolution animal PET imaging of prostate cancer xenografts with three different ^{64}Cu-labeled antibodies against native cell-adherent PSMA. Prostate. 2010; 70:1413–1421. [PubMed: 20687214]

201. Banerjee SR, Pullambhatla M, Byun Y, et al. ^{68}Ga-labeled inhibitors of prostate-specific membrane antigen (PSMA) for imaging prostate cancer. J Med Chem. 2010; 53:5333–5341. [PubMed: 20568777]

202. Elsässer-Beile U, Reischl G, Wiehr S, et al. PET imaging of prostate cancer xenografts with a highly specific antibody against the prostate-specific membrane antigen. J Nucl Med. 2009; 50:606–611. [PubMed: 19289418]

203. Chen Y, Pullambhatla M, Foss CA, et al. 2-(3-{1-carboxy-5-[6-[^{18}F]fluoro-pyridine-3-carbonyl)-amino]-pentyl}-ureido)-pentane-dioic acid, [^{18}F]DCFPyL, a PSMA-based PET imaging agent for prostate cancer. Clin Cancer Res. 2011; 17:7645–7653. [PubMed: 22042970]

204. Holland JP, Divilov V, Bander NH, et al. 89Zr-DFO-J591 for immunoPET of prostate-specific membrane antigen expression in vivo. J Nucl Med. 2010; 51:1293–1300. [PubMed: 20660376]

205. Mease RC, Dusich CL, Foss CA, et al. N-[N-[(S)-1,3-Dicarboxypropyl]carbamoyl]-4-[^{18}F] fluorobenzyl-l-cysteine, [^{18}F]-DCFBC: a new imaging probe for prostate cancer. Clin Cancer Res. 2008; 14:3036–3043. [PubMed: 18483369]

206. Lapi SE, Wahnishe H, Pham D, et al. Assessment of an ^{18}F-labeld phosphoramidate peptido-mimetic as a new prostate-specific membrane antigen-targeted imaging agent for prostate cancer. J Nucl Med. 2009; 50:2042–2048. [PubMed: 19910433]

207. Adams JY, Johnson M, Sato M, et al. Visualization of advanced human prostate cancer lesions in living mice by a targeted gene transfer vector and optical imaging. Nat Med. 2002; 8:891–897. [PubMed: 12134144]

208. Sato M, Johnson M, Zhang L, et al. Optimization of adenoviral vectors to direct highly amplified prostate-specific expression for imaging and gene therapy. Mol Ther. 2003; 8:726–737. [PubMed: 14599805]

209. Zhang L, Adams JY, Billick E, et al. Molecular engineering of a two-step transcription amplification (TSTA) system for transgene delivery in prostate cancer. Mol Ther. 2002; 5:223–232. [PubMed: 11863411]

210. Iyer M, Wu L, Carey M, Wang Y, Smallwood A, Gambhir SS. Two-step transcriptional amplification as a method for imaging reporter gene expression using weak promoters. Proc Natl Acad Sci USA. 2001; 98:14595–14600. [PubMed: 11734653]

211. Sato M, Figueiredo ML, Burton JB, et al. Configurations of a two-tiered amplified gene expression system in adenoviral vectors designed to improve the specificity of in vivo prostate cancer imaging. Gene Ther. 2008; 15:583–593. [PubMed: 18305574]

212. Pouliot F, Karanikolas BD, Johnson M, et al. In vivo imaging of intraprostatic-specific gene transcription by PET. J Nucl Med. 2011; 52:784–791. [PubMed: 21498525]

213. Jiang ZK, Sato M, Wei LH, Kao C, Wu L. Androgen-independent molecular imaging vectors to detect castration-resistant and metastatic prostate cancer. Cancer Res. 2011; 71:6250–6260. [PubMed: 21933883]

214. Sato M, Johnson M, Zhang L, Gambhir SS, Carey M, Wu L. Functionality of androgen receptor-based gene expression imaging in hormone refractory prostate cancer. Clin Cancer Res. 2005; 11:3743–3749. [PubMed: 15897571]

215. Burton JB, Johnson M, Sato M, et al. Adenovirus-mediated gene expression imaging to directly detect sentinel lymph node metastasis of prostate cancer. Nat Med. 2008; 14:882–888. [PubMed: 18622403]

216. Johnson M, Karanikolas BD, Priceman SJ, et al. Titration of variant HSV1-tk gene expression to determine the sensitivity of ^{18}F-FHBG PET imaging in prostate cancer. J Nucl Med. 2009; 50:757–764. [PubMed: 19372484]

217. Johnson M, Sato M, Burton J, Gambhir SS, Carey M, Wu L. MicroPET/CT monitoring of herpes thymidine kinase suicide gene therapy in a prostate cancer xenograft: the advantage of a cell-specific transcriptional targeting approach. Mol Imaging. 2005; 4:463–472. [PubMed: 16285908]

218. Giovacchini G, Picchio M, Briganti A, et al. [11C]Choline positron emission tomography/computerized tomography to restage prostate cancer cases with biochemical failure after radical prostatectomy and no disease evidence on conventional imaging. J Urol. 2010; 184:938–943. [PubMed: 20643445]

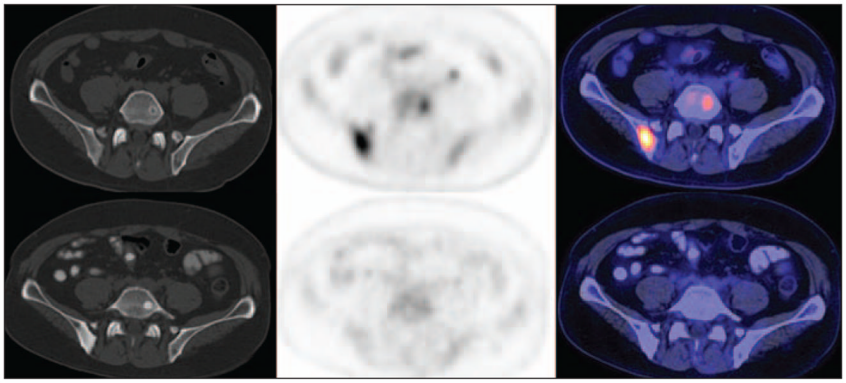

Fig. 1.
60-year-old man. CT (*left*), ^{18}F-FDG PET (*middle*), and fused PET/CT (*right*) images show how androgen deprivation therapy induced decline in FDG uptake in osseous metastatic sites in posterior right ilium and left L5, with concomitant increase in lesion sclerosis. Top panels are pretreatment scans (prostate-specific antigen [PSA] level, 67.4 ng/mL), and bottom panels are posttreatment scans (PSA level, 0.3 ng/mL).

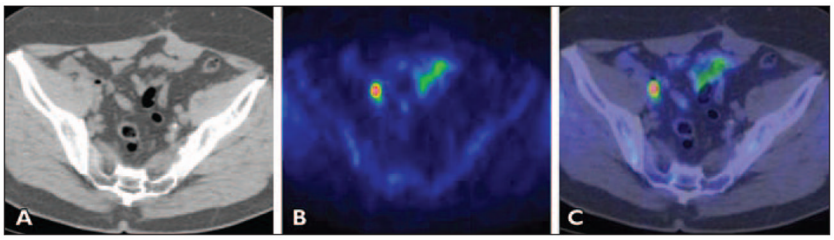

Fig. 2.

Man with biochemical relapse of prostate cancer (prostate-specific antigen [PSA] level, 2.68 ng/mL). **A–C,** CT (**A**), PET (**B**), and fused PET/CT (**C**) images show pathologically increased ^{11}C-choline uptake in subcentimeter right external iliac lymph node. Pelvic lymph nodal area was irradiated with resultant decline in PSA to undetectable level at 3 months after completion of therapy regimen. (Reprinted with permission from [218])

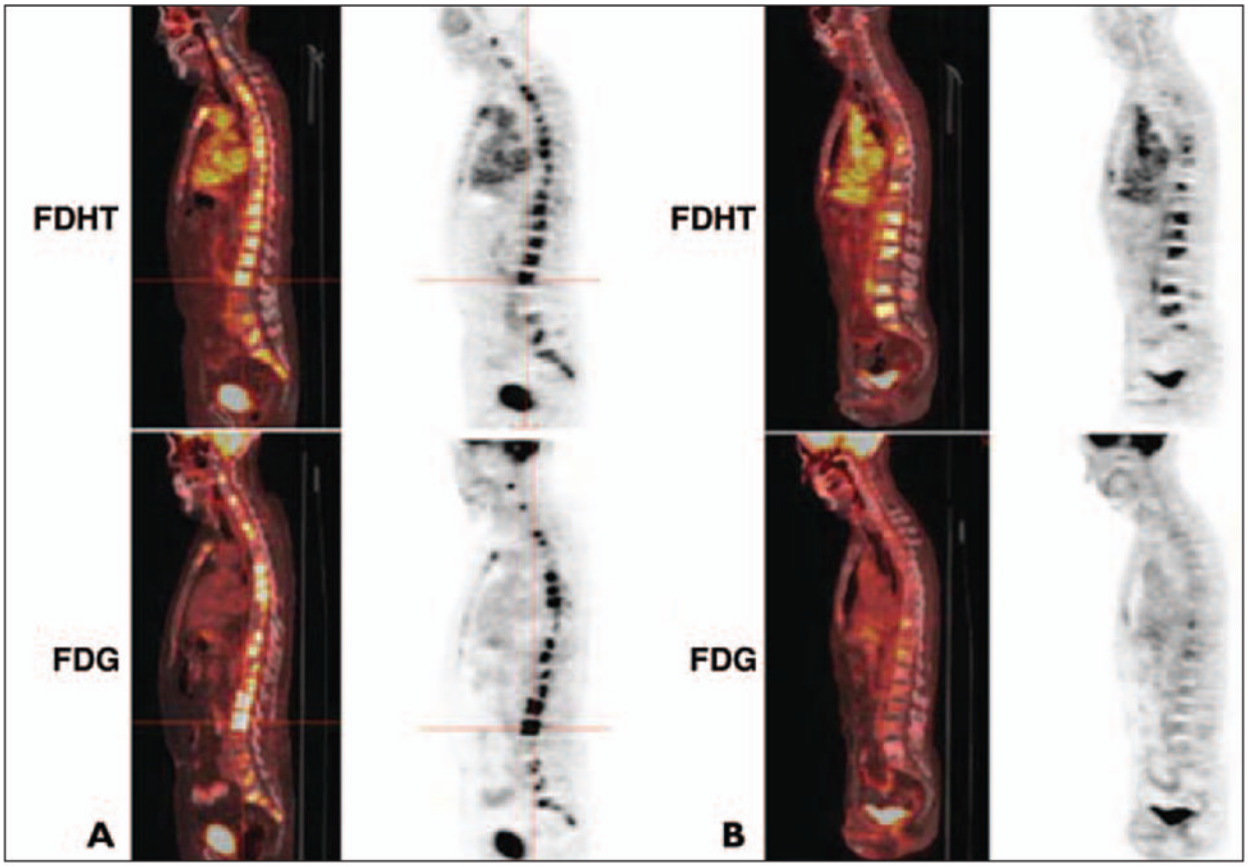

Fig. 3.

Sagittal fused PET/CT and PET images of 16β-[^{18}F]fluoro-5α-dihydrotestosterone (FDHT) (*top*) and FDG (*bottom*) uptake in two different patients with castrate-resistant metastatic prostate cancer.

A, Glycolysis–androgen receptor concordant phenotype.

B, Androgen receptor predominant phenotype. (Reprinted with permission from [47])

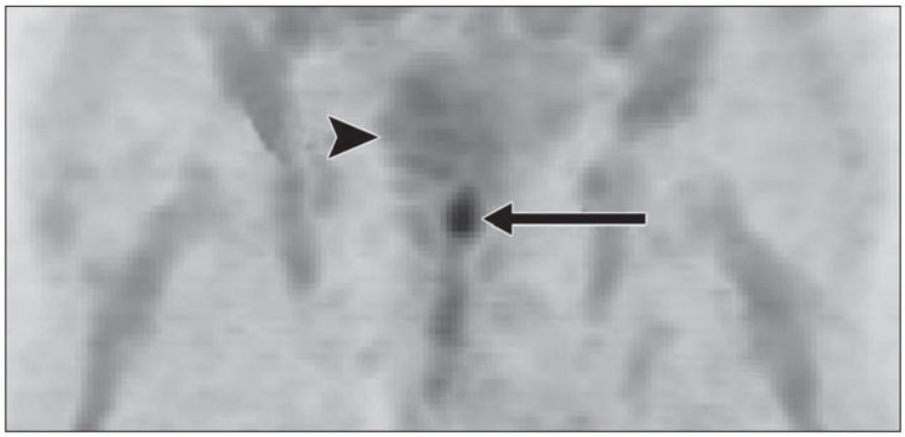

Fig. 4.

71-year-old man with biopsy-proven prostate bed recurrence. anti-^{18}F-FACBC PET maximum-intensity-projection image at 20 minutes shows high uptake in prostate bed (*arrow*) and little bladder uptake (*arrowhead*). (Reprinted with permission from [181])

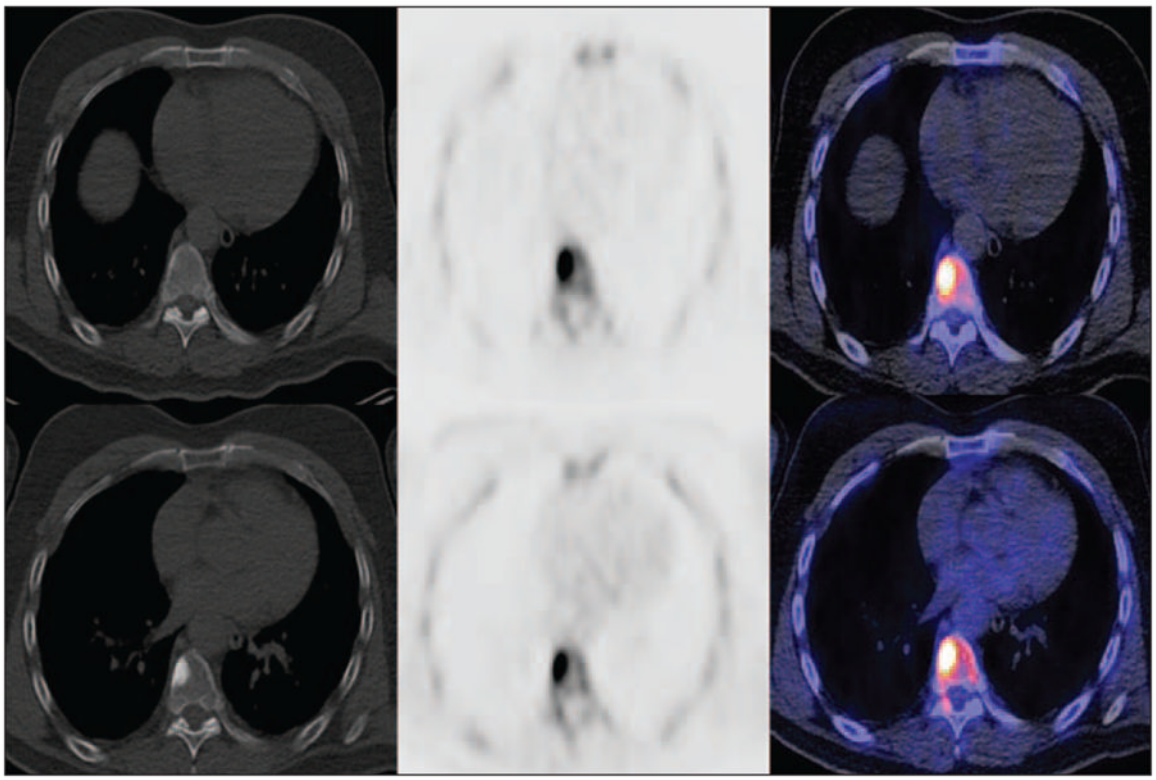

Fig. 5.

54-year-old man with biochemical recurrence of prostate cancer and negative conventional bone scintigraphy. CT (*left*), ^{18}F-NaF PET (*middle*), and fused ^{18}F-NaF PET/CT (*right*) transaxial images show subtle sclerosis at right anterolateral aspect of thoracic vertebral body, which is clearly active on PET before androgen deprivation therapy (*top*) and remains active with increasing sclerosis after 4 months of treatment (*bottom*).